NASA TECHNICAL MEMORANDUM

NASA TM X-2338

NASA TM X-2338

PRELIMINARY ANALYSIS OF AN ATMOSPHERE-ENTRY PROBE MISSION TO JUPITER

by Byron L. Swenson, Larry E. Edsinger, Larry A. Manning, Susan M. Norman, Kenneth F. Sinclair, Alan J. Stratton, and Edward L. Tindle

Office of Advanced Research and Technology
Advanced Concepts and Missions Division
Moffett Field, Calif. 94035

NATIONAL AERONAUTICS AND SPACE ADMINISTRATION • WASHINGTON, D. C. • SEPTEMBER 1971

1. Report No.	2. Government Accession No.	3. Recipient's Catalog No.
NASA TM X-2338		

4. Title and Subtitle	5. Report Date
PRELIMINARY ANALYSIS OF AN ATMOSPHERE ENTRY PROBE MISSION TO JUPITER	September 1971
	6. Performing Organization Code

7. Author(s)	8. Performing Organization Report No.
Byron L. Swenson, Larry E. Edsinger, Larry A. Manning, Susan M. Norman, Kenneth F. Sinclair, Alan J. Stratton, and Edward L. Tindle	A-3826
	10. Work Unit No.
9. Performing Organization Name and Address	130-06-16-07-00-15
Office of Advanced Research and Technology Advanced Concepts and Missions Division Moffett Field, Calif., 94035	11. Contract or Grant No.
	13. Type of Report and Period Covered
12. Sponsoring Agency Name and Address	Technical Memorandum
National Aeronautics and Space Administration Washington, D. C., 20546	14. Sponsoring Agency Code

15. Supplementary Notes

16. Abstract

The preliminary feasibility of depositing an atmospheric-entry probe from a flyby mission to Jupiter has been examined. This report summarizes the scientific, operational, and system requirements and options for the entry mission. In addition, technological problem areas are indicated. These difficulties and uncertainties do not appear to be insurmountable and the mission should receive careful attention.

17. Key Words (Suggested by Author(s))	18. Distribution Statement
Jupiter Entry probe	Unclassified Unlimited

19. Security Classif. (of this report)	20. Security Classif. (of this page)	21. No. of Pages	22. Price*
Unclassified	Unclassified	73	$3.00

*For sale by the National Technical Information Service, Springfield, Virginia 22151

TABLE OF CONTENTS

PRELIMINARY ANALYSIS OF AN ATMOSPHERE-ENTRY PROBE MISSION TO JUPITER

Byron L. Swenson, Larry E. Edsinger, Larry A. Manning, Susan M. Norman, Kenneth F. Sinclair, Alan J. Stratton, and Edward L. Tindle

Office of Advanced Research and Technology
Advanced Concepts and Missions Division
Moffett Field, Calif., 94035

INTRODUCTION

Recently considerable attention has been given to missions to explore the outer planets of the solar system. Many mission modes have been suggested including gravity assisted so-called Grand Tour missions, two planet missions, and single planet missions. The possible modes of exploration include remote measurements from flybys and orbiters and actual in-situ measurements of the atmospheres of the outer planets by probes. The planet which has received the greatest attention for exploration is, of course, the closest of the outer planets, Jupiter.

Jupiter is the largest planet in the solar system and its large mass and low density indicates that its present composition may be very similar to that when the planet was formed. In addition, Jupiter appears to have relative chemical abundances nearly like that of the Sun. For these reasons, a properly instrumented atmosphere-entry probe flown into the Jovian atmosphere could reveal important information on the formation and evolution of Jupiter and of the solar system in general. The purpose of the present paper is to examine in a preliminary way the feasibility of conducting an atmosphere-entry probe mission to Jupiter.

The primary purpose of the mission considered in this report is to deposit a scientific probe into the atmosphere of Jupiter and obtain telemetered data. The telemetry data from the probe will be relayed to Earth by way of the interplanetary bus that will carry the probe to Jupiter. Direct transmission of data to Earth appears overly restrictive.

The scientific requirements will be examined first in analyzing the feasibility of this mission. These requirements will be developed from the rationale of the various measurements relative to accepted planetary exploration goals. A detailed specification of these measurements will then be made. Next, the operational problems and options of the entry mission will be analyzed and a specification of desirable operational profiles presented. The primary purpose of an entry mission is, of course, to measure and reconstruct from those measurements the structure profiles of the atmosphere. The primary errors associated with that reconstruction will be discussed. Finally, a preliminary analysis will be made of the system and booster requirements required to accomplish this mission.

Because of the length of this report, the summary and conclusions of the analysis are presented first and are followed by the details of analysis in the order mentioned. Finally, the suggested mission is described to a depth consistent with the depth of the feasibility analysis.

SUMMARY AND CONCLUSIONS

The preliminary feasibility of depositing an atmosphere entry probe from a flyby mission to Jupiter has been examined. In summary, the mission appears, within the depth of the current analysis, both feasible and attractive. However, there are uncertainties associated with the requirements for survival in the entry thermal environment and the ability to communicate with the probe during terminal descent. In addition, the high deceleration encountered during entry and high trapped radiation environment that must be penetrated will pose difficult development problems for the required instrumentation and electronic equipment. These difficulties and uncertainties do not appear to be insurmountable and the mission should receive careful attention. The most important details of the conclusions are presented below. The complete analysis is presented in the following sections.

1. The reasons for probing the atmosphere of Jupiter are well justified from a scientific point of view. Such measurements have a high probability for information to satisfy recognized scientific goals.

2. Based on current atmosphere models, the added scientific gain of probing below about the 300 bar level appears small. In fact it appears that a design goal of 50-100 bars provides most of the significant scientific returns.

3. Based upon current knowledge of the visible surface of Jupiter, the Equatorial Zone should be probed first and then a near equatorial belt.

4. The most diffficult instrumentation design and operational problems result from the extreme accelerations encountered by the probe and the radiation environment encountered by the flyby bus. Accelerations of 1000 to 2000 g are encountered and a radiation dose of the order of 10^4 rads is expected.

5. The characteristic velocity requirements for this mission, with a 20-day launch window, range from 14.5 to 15 km/sec for good and average opportunities. Titan IIID/Centaur launch vehicles have significant payload capability for such energies. The Centaurs' high departure declinations for some Type I trajectories and KSC range safety constraints require stage coasting in Earth orbit for as much as 40 minutes which is 16 minutes longer than is now possible.

6. Separation analysis indicates that 3σ entry angle errors of $\pm 1.5°$ to $2°$ are present for both the deflected bus and the deflected probe modes of probe separation. If the bus is targeted at periapsis radius of, say, $4R_J$ (as in the case of a Grand Tour mission), entry angles in excess of $-15°$ must be accepted to insure capture during entry.

7. Previous work has shown that survival of the probe through the entry thermal environment to subsonic speeds depends largely on the extent to which the ablation-product vapors block the incoming radiation heating from the shock layer at the extreme enthalpies encountered during entry.

8. It is possible to phase the flyby bus and probe to achieve a line-of-sight relay between them throughout the entry and the required 1-hour descent, within reasonable antenna constraints for flyby periapsis radii between about 1.5 to $5R_J$.

9. The uncertainty in entry angle dominates the accuracy of reconstructing the atmosphere structure based upon measurements of the probe and flyby bus. Considering most of the uncertainties and errors, it appears that the reconstruction of the atmosphere structure can be made to within ±15 km in altitude.

10. The choice of transfer trajectory and entry angle is dominated by the sunlight requirement of the photometer instrumentation on the probe. A Type I transfer trajectory (trip time about 800 days) provides a sunlit side approach, but entry angles steeper than -30° are required to provide sunlight throughout the descent. A 1200-day Type II transfer trajectory provides a dark side approach and entry angles as shallow as -15° may be used. However, an entry of -30° from this trajectory has the advantage of nearly vertical solar lighting during entry and the initial part of the descent. The main disadvantage associated with a -30° entry angle is that a maximum deceleration of about 2000 g may be encountered. The maximum deceleration for a -15° entry is about 1000 g.

Another very important consideration in the choice of entry angles is probe-to-bus communications during entry. It is possible to provide a considerably smaller communications distance when the probe reaches the 100 bar pressure level with a -30° entry than with a -15° entry. Considering all factors including Centaur coast time, trip time, entry acceleration, solar lighting, atmosphere reconstruction accuracy, and communications margin, it is suggested that a 1200-day Type II transfer trajectory be used with a -30° entry angle.

11. The weight and size of the entry probe have been estimated and it appears that the probe will weigh about 250 kg for the deflected bus mode and 300 kg for the deflected probe mode. The required diameter of the probe aeroshell is about 1.5 m.

12. The weight of the flyby bus, which will transport the probe to Jupiter, provide supporting flyby measurements, and relay the data to Earth, was found to be a strong function of the Earth link data rate. For storage and replay of the entry and flyby data at 800 bits/sec the bus weighs about 540 to 870 kg, depending upon the separation mode and flyby science payload. For real-time transmission of the data at 9000 bits/sec the bus weigns about 800 to 1200 kg depending upon the separation mode and the flyby science payload. Thus the total spacecraft weight (probe and bus) ranges from about 830 to 1440 kg depending upon separation mode, data rate, and flyby science payload. The deflected probe mode is suggested because of the higher total system weight required for the deflected bus mode and because there appears to be little advantage in terms of entry guidance uncertainties for this mode.

13. The payload and characteristic velocity requirements of this mission require a Titan IIID/Centaur launch vehicle. It appears that a five segment Titan IIID can be used with some payload margin if storage and replay of the entry and flyby data are acceptable. The Burner II may be required as an upper stage to open the launch window for the more difficult launch years. A seven segment Titan IIID is required if real-time transmission of data is required. The Burner II upper stage will not appreciably open the launch window for the seven segment Titan IIID combination and very little payload margin is available for the difficult years.

SCIENCE REQUIREMENTS

The scientific need for an atmosphere-entry probe of Jupiter will be developed by discussing the pertinence of understanding various Jovian phenomena in view of generally accepted planetary exploration goals. Following this will be a description of the measurable quantities that characterize Jovian phenomena. The final portion will be definitions of the instruments needed to implement the measurements and of the spacecraft system needed to support and transmit the data.

Science Rationale

The 1965 study of the NAS Space Science Board (ref. 1) concluded that the nation's total planetary program should be designed to increase our understanding of: (1) the origin and evolution of the solar system, (2) the origin and evolution of life, and (3) the dynamic processes that shape man's terrestrial environment. Since the validity of these scientific goals is generally recognized, any discussion of the scientific rationale for an outer planet mission should consider the relationship between the detailed scientific objectives of the mission and the planetary program goals. This discussion will outline some of the contributions that scientific data from an atmosphere-entry probe mission can make toward the planetary program goals.

A 1969 study by the Space Science Board entitled, "The Outer Solar System: A Program for Exploration" (ref. 2) recommended eight prime scientific objectives for exploration of the outer solar system. The three that relate to the kinds of data obtainable from atmospheric entry probes are: (1) determine the chemical and isotopic composition of the atmospheres of the outer planets, (2) determine whether biologically important organic substances exist in these atmospheres and characterize the lower atmospheric environments in terms of biologically significant parameters, and (3) describe the motions of the atmospheres of the major planets and characterize their temperature, density, and composition structure.

The first objective bears on the origin and evolution of the solar system. A major problem facing all theories of the origin of the solar system is determination of the chemical composition of the Sun and the planets. The present evidence is based on determinations of the composition of the Sun, the Earth's surface, and meteorites. These compositions do not agree. Available evidence suggests that Jupiter (and perhaps Saturn) may have retained all elements in its original relative abundances and thus may be more like the primitive solar system in composition.

The hydrogen-to-helium abundance ratio of Jupiter is of particular interest since it has significance for more general cosmological problems. Rival theories of the origin of the universe differ in the amounts of helium they predict for bodies of various ages in the universe. The determination of the hydrogen and helium abundance for Jupiter would thus provide evidence bearing directly on the validity of alternative cosmological theories.

The second objective will contribute to understanding the origin and evolution of life. It has been fairly well established that conditions on the primitive Earth were very different from those of today. It is generally believed, with some disagreement over the details, that the early terrestrial atmosphere was highly reducing and consisted primarily of methane and ammonia. The formation of complex organic molecules in this environment is believed to have resulted from chemical

reactions stimulated by solar ultraviolet radiation, atmospheric electrical discharges, and local sources of endogenic thermal energy.

It is known that the atmosphere of Jupiter is similar in many respects to this model for the primitive Earth. Thus a logical first step in the biological exploration of the outer planets is the investigation of the atmosphere of Jupiter to determine how favorable conditions there are for the abiogenic formation of organic compounds. Questions of interest include: Are there warm regions in the lower atmosphere? Are electrical discharges present? What solvents are available? What chemical reactions are occurring in the upper atmosphere? The next step in sophistication is a search for the complex organic substances themselves.

The final objective will contribute to the third planetary program goal which is concerned with understanding processes acting in the terrestrial environment. While the atmosphere of Jupiter differs greatly from that of Earth, the re-examination of fundamentals needed to embrace a different system could lead to new ideas of importance to terrestrial meteorology. This has occurred from investigations of other planets. For example, recent developments in the study of the atmosphere of Venus have led to a new understanding of the circulation regime originally proposed many years ago by Hadley (ref. 3) for the Earth, and current work on the diurnal circulations on Mars is leading to a fresh appreciation of diurnal effects in terrestrial boundary layers.

Although the data obtainable from an entry probe will relate more directly to atmospheric structure than to circulation, all other data obtained through remote sensing of the atmosphere have to be interpreted in terms of a model representing physical and chemical conditions in the atmosphere. Establishing an accurate model of the atmosphere composition and structure through direct measurements by an entry probe will thus provide a basis for unraveling and interpreting data obtained from future Earth-based, flyby, and orbiter experiments.

Measurement Specification

Based on the foregoing, a set of measurement specifications for a Jupiter atmosphere-entry probe mission is presented here. The choice of physical parameters to be measured is consistent with the 1969 Space Science Board outer solar system scientific objectives discussed previously. Measurement accuracies and sampling intervals have been specified for some of the parameters in order to facilitate the analysis of probe subsystems that are sensitive to such specifications. The values selected are believed to represent reasonable choices but it should be kept in mind that they were selected in large part subjectively without the benefit of detailed analysis. It should also be noted that some aspects of the discussion depend on the atmosphere structure model assumed for the study[1] and on the assumed cloud layer/composition model of Lewis (ref. 4). In addition, desirable measurements are specified in this section of the report without too much consideration for the feasibility of obtaining those measurements with an atmosphere-entry probe. Actual feasibility is discussed in the section "Instrumentation Requirements."

Of course, it is desirable to obtain pressure, density, and temperature profiles along with the abundance of the major constituents for the entire atmosphere. Probably the most important parameter from a cosmological point of view is the ratio between the abundance of hydrogen and

[1] A more detailed discussion of the atmosphere model is presented later in this report.

helium. The distribution of positive ions in the upper atmosphere should also be determined. Measurements of the various profiles above the tropopause should be made at least every 10 km.

The lower atmosphere is characterized by many apparent cloud layers. According to Lewis' atmosphere model (ref. 4), the bases of thermodynamically likely cloud layers are:

NH_3 (solid)	$T \cong 180°$ K, $P \cong 8$ bars
NH_4SH (solid)	$T \cong 225°$ K, $P \cong 15$ bars
H_2O (liquid and solid)	$T \cong 300°$ K, $P \cong 40$ bars
NH_4Cl, some NH_4Br, NH_4I	$T \cong 475°$ K, $P \cong 250$ bars
SiO_2 + other oxides	$T \cong 1600°$ K, $P \cong 5 \times 10^4$ bars

An attempt to reach the SiO_2 cloud base is clearly out of the question. The base of the NH_4Cl cloud layer is the next logical goal; it calls for a probe capable of surviving to a T of about 500° K and 300 bars pressure. On the basis of Lewis' model there is no great advantage in going deeper unless one goes very much deeper. Thus a 1000 bar probe would not offer a decisive advantage over a 300 bar probe.

If 500° K, 300 bar conditions are too difficult, the 300° K, 50 bar level represents the next best choice. This would reach the base of the H_2O clouds in Lewis' model. If this level is not achievable, the probe should be designed to come as close to it as possible.

Pressure, density, and temperature profiles should be determined below the tropopause with measurements made at least at every kilometer. The pressure range is from about 0.1 bar to the design survivability limit. The temperature range is from about 50° K to as much as 550° K for the 300 bar pressure level.

The abundance of atmospheric gases as a function of altitude is needed. Equilibrium constituents likely to be present at the 300° K level in concentrations greater than 1 ppm are, in order of decreasing concentration, H_2, He, H_2O, CH_4, NH_3, Ne, H_2S, Ar. Determination of a composition profile, along with P and T profiles, will provide indirect evidence bearing on cloud composition and location. A sampling interval of 10 km or so is desirable.

Direct measurements on the clouds themselves should include at least approximate upper and lower bounding altitudes, if well defined, and gross cloud chemical composition. Also desirable would be information on particle number density vs. altitude, particle size vs. altitude, and cloud chemical composition vs. altitude. Finally, the isotopic abundance ratios of H/D, $^3He/^4He$, $^{36}Ar/^{40}Ar$, and $^{13}C/^{12}C$ should be determined.

Entry Location

The following points should be considered with regard to the location on Jupiter to which a probe should be targeted. Data from the first probe mission should be as representative as possible of the whole planet, and should be from a region that is readily observable from Earth. Thus the first probe should be targeted for the region, say, between 30° N and S latitudes, excluding the Great Red Spot and other less permanent anomalous regions. Within this region a belt (dark band) or a zone (light band) must be chosen. The recent report of 5μ brightness temperatures up to

300° K associated with dark areas of the North Equatorial Belt (ref. 5) may be viewed as evidence of an absence of high level clouds within the darker areas. In order to sample the cloud structure, then, a target point within a zone should be selected for the first probe. The Equatorial Zone, with boundaries in the range 7° N ± 2° and 7° S ± 2°, is probably the best choice for the first probe even though the apparent rotation period of this region is atypical with respect to the rest of the planet. The North Tropical Zone, highly variable in width and location (between 15° and 30° N), and the South Tropical Zone, with an average width of about 10° and location between 17° and 30° S, are possible alternate target areas for a first probe.

Since a complete entry probe mission program may well include more than one spacecraft, other targeting areas should also be considered. Entry into a belt region is favored for a second probe mission since zones and belts comprise the typical gross visible structure of Jupiter between 45° N and S. Entry into the North Equatorial Belt (width 1°-15°, located between 6° and 20° N) would allow sampling of a region with the most distinct variation from conditions in the zones if the interpretation of Westphal's 5μ data is correct. Entry into the south component of the South Equatorial Belt (average width about 5°, located between 12° and 20° S) would provide data from a belt region at the same latitude as the Great Red Spot.

If a third spacecraft probe is available, it is recommended that it be targeted for the Great Red Spot (covering 20°-40° of longitude, 10°-20° of latitude, and centered at about 22° S). This anomalous region is of great interest from the points of view of both atmospheric dynamics and possible biological conditions. Plausible targets for a fourth probe include the North Polar Region (located above 48° N; the South Polar Region boundary is usually at a substantially higher latitude) or the South Tropical Zone. There is evidence that the top of the cloud layers is appreciably lower in the polar zones than in the latitudes between 45° N and S, indicating the possibility of a subadiabatic region in the polar zones (ref. 6). The South Tropical Zone is of interest since the Great Red Spot is located partly within it.

A fourth probe to the South Tropical Zone would form an attractive combination in conjunction with the third to the Great Red Spot itself and the second to the south component of the South Equatorial Belt. With the first probe to the Equatorial Zone, this combination would provide sampling of two zones, one belt, and the Red Spot with the belt and one of the zones adjacent to the Red Spot. On the other hand, probes to the Equatorial zone, the North Equatorial Belt, the Great Red Spot, and the North Polar Region would allow for sampling of four distinct regions, including those for which there is some evidence of substantial variations in cloud levels and atmospheric structure.

In summary, two plans are suggested for targeting the four probes:

	Target	
Probe	*Plan A*	*Plan B*
1	Equatorial Zone	Equatorial Zone
2	South component of South Equatorial Belt	North Equatorial Belt
3	Great Red Spot	Great Red Spot
4	South Tropical Zone	North Polar Region

Instrumentation Requirements

Science payloads for this mission are included both on the probe and the flyby bus. The bus experiments are intended to complement the direct measurements made by the probe during entry by providing redundant and supporting data. These two experiment sets are designed generally to meet the science objectives and measurement requirements outlined above. In some cases, it was not feasible to measure either directly or indirectly some of the previously discussed atmosphere parameters with an atmosphere-entry probe. Instruments composing each payload set are discussed below. Each instrument is described briefly and problem areas or development requirements are identified. Finally, additional experiments of reasonably significant value over and above the baseline experiments are delineated for inclusion on the flyby bus if payload considerations permit.

Probe instrumentation - The probe experiments are designed to provide data on the variations of physical parameters of Jupiter's atmosphere with altitude and the constituent composition and vertical distribution of the clouds. The probe experiments are summarized in table I and discussed briefly here.

The structure of most of the Jovian atmosphere can be inferred from measurements of deceleration, temperature, and pressure. The measurement of deceleration can be used to obtain the ratio of temperature to mean molecular weight and that combined with a measurement of temperature would allow the calculation of mean molecular weight. At the very upper reaches of the atmosphere (over 100-200 km above the cloud tops, ref. 7), however, hydrogen and helium are assumed to be in diffusive equilibrium. That is, the concentration gradient of each constituent is determined independently by an equilibrium between the self-diffusion (both due to the concentration gradient and the thermal gradient) of that constituent and the effects of gravity. Thus two independent and coincident scale heights are established and the overall Jovian hydrogen-to-helium ratio cannot be determined at high altitude.

At altitudes over 50 km above the cloud tops, the probe is highly hypersonic. It will be difficult to infer the ambient pressure from a pressure measurement at the probe stagnation point because of the unknown gas composition and the extreme enthalpy of the shock layer. Temperature measurements at this enthalpy are impossible. However, the deceleration history during this flight region can be related to atmospheric density if the drag coefficient of the vehicle, its mass, and the vehicle velocity are known. The measured accelerations are integrated to determine the instantaneous velocity.

In addition to density, the accelerometer measurements are used to determine static pressure by integration of the barometric equation. Altitude is determined by integrating the vertical component of velocity assuming that the flight-path angle is known and that a suitable reference altitude can be established. The ratio of temperature to mean molecular weight can be established from the ratio of pressure to density. A temperature profile can then be calculated using this ratio and the mean molecular weight of the atmospheric gas mixture obtained from low-speed lower altitude pressure, temperature, and acceleration measurements and from mass spectrometer data. For this part of the entry trajectory, measurements are required at least every 10 km.

For the subsonic region, from about 50 km above the cloud tops to the maximum probe depth, direct measurements of pressure and temperature would be made in addition to continuing acceleration measurements. In this region measurements should be obtained every kilometer. The

equipment required for these functions is available and should pose no major technological difficulties. The major difficulty with this experiment is determining the instantaneous flight-path angle of the vehicle during the hypersonic part of the entry and establishing a suitable reference altitude to start the integration (either upward or downward). These difficulties will be addressed in greater detail and an analysis of the expected accuracy of the accelerometer experiment will be presented in the section "Atmosphere Reconstruction."

The photometer experiment included in the probe payload package is designed to: (1) sense the cloud tops, (2) detect atmospheric aerosols, (3) detect lightning, (4) determine abundance of methane and ammonia, and (5) determine the H/D ratio. To detect lightning, the photometer, of course, looks down while the other tasks require an upward looking photometer. The upward looking photometer requires a sunlight entry situation for the probe. A wavelength interval is used in which there is no atmospheric absorption and the cloud tops are sensed by a sudden drop in the solar illuminance.

Atmospheric aerosols can be inferred by a gradual decrease in the solar illuminance. By observing several different wavelengths it may be possible to decide whether Mie or Rayleigh scattering is occurring and, consequently, estimate particle size.

Lightning flashes can be observed by a downward looking sensor. The design used should discriminate against steady or slowly varying light so that only transient light sources having a time-intensity pattern typical of lightning flashes will be recorded.

The abundance of an atmospheric constituent can be determined by measurements in absorption bands characteristic of the molecule being sought. Useful wavelengths for methane are 6,800 Å, 8,400 Å, and 10,900 Å; for ammonia, 9,950 Å, 7,950 Å, and 5,510 Å; and to determine the H/D ratio, the abundance of CH_3D can be monitored at 4.55μ. Independent measurements required for data interpretation include solar flux and a pressure and temperature profile.

The instrumentation required to perform these functions is relatively straightforward and requires small space, weight allowance, and power. Since the first two measurements discussed above (cloud tops and aerosols) can use the same sensors, a maximum of six channels would be required to perform the measurements outlined. Measurements should be obtained every kilometer in each channel from about 50 km to the end of the descent.

The gas chromatograph/mass spectrometer is intended to provide data on the elemental, molecular, and isotopic composition of the atmosphere. The gas chromatograph is used to assist in resolving the ambiguities in the mass spectrometer data and to increase the effective dynamic range of the mass spectrometer so that trace constituents can be detected.

The range of molecular mass to electron charge ratio of the spectrometer should extend to 60 so that complex or higher weight inorganic species (CO_2, H_2Se, COS, etc.) and organic molecules can be detected.

Sample processing time should be such that a resolution of about 10 km can be achieved from about 50 km above the cloud tops to end of probe life. The present state of the art will permit a processing time of 2 to 5 minutes.

Bus instrumentation The bus experiments are primarily directed toward gathering synoptic data over the planet and supporting the probe experiments. The bus experiments are summarized in table 2 and discussed below. The baseline experiments are covered first followed by a brief discussion of the other desirable, but lower priority, experiments. The imaging experiment should be designed to provide resolution at the cloud tops ranging from that achievable from Earth (~1500 km) down to about 10 km at closest approach. The imagery obtained from such a system should provide valuable information about cloud structure, circulation, and distribution. Since the nature of the band and belt structure is variable, the imagery should give detail of the actual nature of the entry site which will help interpret the photometer experiment on board the probe.

The far encounter picture taking sequence will begin at a distance of about 30 Jovian radii at a frame rate of one every 30 minutes. This mode of operation will continue until $10R_J$, the limit for full disk frames, and then the frame rate will be increased to one every 2 minutes until the field of view crosses the terminator at which time the picture taking sequence will stop.

The camera requirements, with the exception of lifetime considerations, are quite modest and well within the state of the art. A 400 X 400 line system with 6-bit grey scale encoding and a field of view of 6° is required. Provided that reliability is not seriously compromised, a filter wheel with several filters from the near ultraviolet to the near infrared should be provided.

The discrepancy between the apparent absorbed solar energy at Jupiter (about 50%) and the observed brightness temperature (about 130° K, ref. 8), suggests some internal heat source at the planet. The IR radiometer experiment is designed to determine whether or not this discrepancy is real by making more accurate temperature measurements than are possible from Earth. In addition, the radiometer will provide data over its spectral band regarding the temperatures in the probe entry region.

The instrument field of view should be about 1° and data should be acquired every 30 seconds to provide essentially contiguous coverage at closest approach. While this sampling period is somewhat wasteful because of overlap at far distances from the planet, the data production rate is still low enough that additional programming for the device appears to be unwarranted. The wavelength for maximum emission at the surface temperature of Jupiter falls in the range 20-25μ. Consequently, it is desirable to use a detector that functions effectively up to 25μ. The requirements for the radiometer are well within the state of the art and the only complication is a requirement for detector cooling (about 80° K) during operation in order to have an adequate signal-to-noise ratio at the anticipated measurement temperature.

An ultraviolet photometer experiment is included in the bus science payload to complement the measurement of hydrogen to helium ratio by the entry probe and to complement the data obtained by radio occultation. The mode of operation of this instrument is identical to the mode described for the IR radiometer since the UV photometers field of view is also 1°. It detects hydrogen and helium by observation of the resonance reradiation at 584Å and 1216Å, respectively. This device is well within the state of the art and the instrument has the virtues of being very light and consuming little power.

The objective of the RF occultation experiment is to obtain information on the mean molecular weight, temperature, and scale height of the Jupiter atmosphere as well as information on the planet's ionosphere and the electron density in interplanetary space. The atmospheric data

obtained by RF occultation will complement greatly the probe atmosphere density and composition measurements. The basic data required for this experiment are frequency, phase, and amplitude changes in the signals received from Earth as functions of spacecraft position. Refraction of the radio signal by the planet's atmosphere produces an apparent change in the motion of the spacecraft. With the data outlined above and knowledge of the position of the spacecraft, the magnitude of the refraction can be ascertained. With independent knowledge of the atmospheric composition, the basic experiment objectives can be attained.

For the ionospheric and interplanetary electron density measurements, a two-frequency system is required to permit comparison of the phase advance and group delay of the two signals. In this way the integrated electron density and its variation with time can be determined. During encounter, one 8-bit sample per second should be sufficient. Data production over other parts of the trajectory will be considerably less.

The equipment requirements for this experiment are nominal. The basic S-band system is used for the occultation measurements, requiring no additional spacecraft equipment. The two-frequency system requires a small low power receiver aboard the spacecraft.

Jupiter seems to have a very interesting local particle and field environment. An experiment has been included to determine the extent, intensity, and distribution of this environment and, in addition, to provide data that may permit a better understanding of the nature and origin of the decimeter and decameter radio noise emitted by Jupiter. Based on present models, magnetic field intensities as high as several gauss and electron population densities of the order of 10^7 electrons/cm^3 at 3 radii should be expected during the flyby.

Adequate spatial resolution can be obtained with a measurement rate of one sample per second from about 30R_J on approach to a similar distance after encounter. Interplanetary measurements can be taken at a much lower rate.

If payload provisions permit, a series of additional experiments have been defined which are significantly valuable but of lower priority than those described above. These experiments include infrared (IR) and UV spectrometry, very low frequency reception, and topside sounding.

The IR spectrometry measurements would make it possible to study polyatomic and organic molecules in the atmosphere and the UV measurements would provide data on atoms, diatomic molecules and, to a limited degree, organic molecules in the atmosphere. Both instruments should have a field of view of about 1° and a scan rate of about 1 scan every 30 seconds. Measurements would be made from about 10 radii and continued past the dark side.

Very low frequency electromagnetic waves may be generated by electrical discharges in the lower atmosphere, such as lightning, and perhaps other sources including auroras. The identification of such waves at Jupiter would indicate the existence of low altitude electrical disturbances. Such measurements would also provide ionospheric data that, when coupled with other information, could provide some insight into the characteristics and behavior of the ionosphere. The very low frequency device is essentially a simple low frequency receiver with a coil type antenna. The data it collects would be digitized and stored for transmission. Some means should be provided to correlate the data with probe photometry.

The topside sounder would provide data on the ionosphere electron density profile as a function of altitude. Both dark and light side measurements should be obtained to provide information on the diurnal variation of ionosphere properties. The reflection frequency, f, for a given electron density, n, is given by

$$f = 8.97 \times 10^3 \sqrt{n}$$

To cover a reasonable electron density range, measurements should be performed over the range of 3-50 MHz. Useful data could be obtained from one or more profiles under both light and dark conditions and, to conserve power, the data should be taken in the vicinity of closest approach. Data rates are low and the device is relatively simple and lightweight. The long antenna required may be a serious problem, however.

Finally, consideration must be given to the vulnerability of the instrumentation to environmental effects. Since the bus and probe trajectories penetrate the Jupiter radiation belts, shielding must be provided to keep the accrued dose to a reasonable level. It has been assumed here that most of the electronic circuitry and components will tolerate a dose as high as 10^4 rads without serious transient or permanent effects. Photomultiplier tubes, vidicons, and other sensitive components should have at least an order of magnitude greater protection but, in any case, will probably exhibit serious transient effects. The magnetic field anticipated is also likely to cause serious effects in phototubes, vidicons, and similar components although magnetic shielding can be provided to minimize these problems. To insure some data acquisition in the event that the radiation environment is much more severe than anticipated, the bus experiments should all be operating before the belts are reached.

OPERATIONS ANALYSIS

This section is an analysis of the operational problems and options of an atmosphere-entry probe mission to Jupiter constrained by the science requirements discussed in the previous section. The operational areas of principal interest lie in the two general areas of heliocentric trajectory selection and mission targeting. The general area of mission targeting includes all the highly interactive operations within the sphere of influence of Jupiter. This includes approach separation, atmosphere entry dynamics and thermodynamics, relay communications geometry, and entry targeting including solar lighting requirements.

Heliocentric Trajectory Selection

Two launch opportunities were selected for this study, 1978 and 1981. These years are representative of the trip time – characteristic velocity (V_C) relationships associated with launch in a nominal (average velocity requirements – 1978) and a good (low requirements – 1981) launch year. In addition, these years are in a time period when a first generation entry probe into the atmosphere of Jupiter could possibly be launched.

Tabular heliocentric transfer trajectory data for the 1978 and 1981 launch opportunities are presented in tables 3 and 4, respectively. These data are for the minimum velocity transfers for

various discrete trip times and include information on launch and arrival dates and vectors. The characteristic velocities (V_C) for these transfers are summarized in figures 1(a) and 1(b). These figures also show the additional ΔV required to obtain a 20-day launch window as indicated by the dashed curve. The cusp in figure 1(a) (1978) occurs for transfers with heliocentric transfer angles near 180°. Jupiter is not exactly in the ecliptic plane so the V_C increases near 180° transfer angles because of the out of plane effects. In 1981, a similar phenomenon occurs but the increase in V_C is barely noticeable because Jupiter is very near its node (0° heliocentric latitude) for the arrival dates associated with near 180° transfers. It can also be seen from figures 1(a) and 1(b) that characteristic velocity requirements for 1978 (a nominal opportunity) and for 1981 (a good opportunity) are about 15 and 14.5 km/sec, respectively. For both launch years attractive transfer trajectories occur near 800 days trip time for Type I transfers and at near 1200 days for Type II transfers.

The other trajectory parameter of principal interest for Earth departure is the departure declination of the hyperbolic asymptote. The departure declinations available for launch from KSC are limited by range safety azimuth constraints and by the allowable coast time in the departure parking orbit. For the departure energy requirements shown in figures 1 and 2, most of the launch vehicle combinations that have reasonable capability utilize the Centaur upper stage for all or part of the hyperbolic insertion maneuver. The Centaur stage is, however, currently limited in orbital coast time to about 24 minutes (ref. 9) by several system design considerations. The departure declinations achieved as a function of coast time for various launch azimuths within range safety constraints of KSC are indicated in figure 2. These data are for a departure excess speed, V_∞, of 0.3 emos which is typical for the transfer trajectories under consideration. It can be seen that negative departure declinations up to -50° can be achieved for coast times under 1/2 hour. However, positive departure declinations greater than 30° require orbital coast times in excess of 40 minutes.

The required departure declinations for minimum energy transfers for the 1978 and 1981 launch opportunities are summarized in figures 3(a) and 3(b). It can be seen that departure declinations in excess of 25° are required for the short trip-time Type I transfers during the 1978 opportunity. The long trip Type II transfers (transfer angles greater than 180°) have departure declinations between 0° and 10°. During the 1981 opportunity the departure declinations for both Type I and Type II trajectories are bounded between -10° and 10°.

Examination of launch opportunities during an entire cycle of Jupiter oppositions indicates that 5 opportunities out of 13 require Earth departure declinations in excess of 10° and these are always for Type I transfers. If missions are to be sent to Jupiter along Type I trajectories in such years (as in 1979 and 1980) then the Centaur coast time limit must be increased to as much as 40 mimutes. The 1980 opportunity is the last such opportunity prior to 1989.

Mission Targeting

As stated earlier, the general area of mission targeting includes the highly interactive operations within the sphere of influence of Jupiter. The particular operations are all highly coupled and many iterations were required to arrive at an understanding of the major impacts and a choice of a targeting specification.

This discussion will start with the approach guidance problem. Separation analysis has indicated the feasibility of two approach modes: (1) the deflected bus mode where the bus and probe are targeted for entry and, at some distance prior to entry, the probe is separated and the bus is deflected to an appropriate nonimpacting trajectory, and (2) the deflected probe mode where the bus and probe are targeted along an appropriate nonimpacting trajectory and, at some distance prior to encounter, the probe is separated and deflected onto an impacting trajectory. Since each mode has its peculiar advantages and disadvantages, both modes were carried throughout the subsequent analysis.

The discussion will then proceed to the area of atmosphere-entry dynamics and thermodynamics along with the terminal descent time required to reach required atmosphere pressure levels. Based primarily upon this descent time, the relay communications geometry problem will be examined for its impact on the deflection maneuver and the choice of periapsis altitude for the flyby bus. Next the area of entry targeting will be discussed where the constraints imposed by some of the science requirements (such as solar lighting) are examined. Finally, the major operational impacts will be summarized and a specification of targeting for the mission will be given.

Separation analysis– For the deflected bus mode, the bus is separated from the probe and deflected onto a nonimpacting trajectory to provide a relay communication system. The targeting error at entry results from the imperfect capability of the navigation system to determine the spacecraft position and the capability of the on-board midcourse control system to minimize the projected error at vacuum periapsis. The accuracy with which the target vacuum periapsis radius must be controlled is a function of the allowable entry-angle dispersion and the value of the entry angle itself.

The target vacuum periapsis radius is shown as a function of entry angle in figure 4 for a typical hyperbolic approach speed. Entries at very shallow entry angles from 0° to -3.6° are not of interest since the probe will not encounter enough deceleration and will skip out of the atmosphere. For shallow entry angles near the skipout boundary the slope of the curve presented in figure 4 indicates that a 200-km error in the projected altitude of the vacuum periapsis will result in a 1° error in entry angle. For target entry angles of -15° that same error in periapsis altitude will only make an error in entry angle of about $1/3^\circ$. It is projected that an accuracy of about 300 km in periapsis radius can be achieved to a 1σ level by the Deep-Space Network (DSN) system where tracking to within 10 days of the time of encounter is utilized, making the 1σ entry angle error at -15° about $1/2^\circ$. Additional improvements in the DSN system, tracking to within, say, two days of encounter, or inclusion of an on-board terminal guidance system could reduce this dispersion (ref. 10). The conclusion, from a guidance point of view, is that entries can be made with confidence (i.e., to 3σ) as shallow as 3° steeper than the skipout boundary if a deflected bus mode is used and if separation occurs 6 to 10 days before entry. Somewhat lower entry angle dispersions occur for steeper entries.

For the deflected probe mode, the probe is separated from the bus, which is on a flyby trajectory, and is deflected onto an impacting trajectory. The principal source of entry angle error for this mode is the separation maneuver with the position error of the spacecraft being a second-order effect. The separation maneuver error has two components: (1) the error in the magnitude of the applied velocity increment and (2) the error in its direction. 1σ errors of 1 percent in magnitude and 1° in direction are typical for this maneuver; of these errors, the magnitude error predominates. This is shown in more detail by the following analysis.

Figure 5 shows that, as the spacecraft approaches Jupiter along a trajectory targeted to fly past the planet at a periapsis radius r_p, the probe is separated at a distance r_S with a velocity impulse ΔV to place it onto an impacting trajectory targeted to enter the atmosphere at an angle γ_e. The error in magnitude of the velocity increment primarily changes the deflection angle $\Delta\gamma$ and only to second order changes the energy of the impacting trajectory. The error in the direction of the velocity increment, on the other hand, primarily changes the energy of the impacting trajectory and only to second order changes the deflection angle $\Delta\gamma$. Both errors contribute to an error in the resulting entry angle. A complete mathematical development for the calculation of these errors is presented in appendix A.

Equation (A4) of appendix A has been used to calculate entry angle errors for a 1σ error of 1 percent in the magnitude of the deflection velocity increment as a function of entry angle for several flyby periapsis radii and several separation distances. The results of those calculations are presented in figure 6. The first point to be noted from figure 6 is that the entry angle error is nearly independent of the separation radius, r_S. This is caused by the compensation between the longer time for errors to propagate at larger separation distances and the smaller deflection velocity requirements and hence smaller error at larger separation distances. Second, it should be noted that the entry angle error decreases rapidly for increasingly steeper entries and for decreasing flyby periapsis radius.

Equation (A6) has been used to calculate entry angle errors for a 1σ error of 1° in the direction of application of the deflection maneuver as a function of entry angle for several flyby periapsis radii and several separation distances. The results of those calculations appear in figure 7. First, it should be noted that the errors in entry angle due to a typical error in the direction of the deflection velocity increment are of the order of half that due to a typical error in the magnitude of that velocity increment. Second, the error due to direction is a strong function of separation distance and decreases rapidly with increasingly steeper entries.

In order to determine the total error in the entry angle for the deflected probe mode, the error due to an error in deflection increment magnitude must be root-sum-squared with the error due to direction. The resulting 3σ RSS error is shown in figure 8. In order to insure to a 3σ probability a successful entry must be targeted steeper than the skipout limit (i.e., $\gamma_e = -3.6^\circ$) by an amount equal to the 3σ dispersion for that targeted entry angle. The permitted entry region is thus to the right of the shaded region in figure 8. The primary parameter of importance in limiting the choice of entry angle is the flyby periapsis radius. Separation radius appears to have a very minor effect. If the flyby periapsis radius is as small as $1.1R_J$, then target entries as shallow as -5° may be attempted. However, if the periapsis radius is selected at near $4R_J$, then target entry angles steeper than -15° must be accepted.

Atmosphere entry dynamics— Before the flight dynamics of an entry probe into the Jovian atmosphere can be discussed, the various postulated atmosphere structures and compositions must be considered. Several atmosphere models have been published (refs. 7 and 11-15). Each is based on interpretations of the rather meager Earth-based spectrometry and radiometry measurements. The range indicated for the density-temperature profiles of each of these models is shown by the shaded region in figure 9. The only model that lies outside this shaded band is that indicated by the dashed line.[2]

[2] "Warm Extended Atmosphere," Jet Propulsion Lab., 1970 (unpublished).

For the purposes of analysis, three model atmospheres (a nominal and two extremes) were chosen from the various references. The nominal model, referred to hereafter as model B, is composed of the model of reference 13 above the cloud tops and the Lewis model B (ref. 11) below the cloud tops. In figure 9, model B lies in the middle of the shaded area above the tropopause and on the lower side of the shaded area below the tropopause. A lower density model referred to hereafter as model A, is composed of the model of reference 15 above the cloud tops and the Lewis model A (ref. 11) below the cloud tops. A high density extreme model, referred to hereafter as model C, is the JPL model. All models were references to a cloud top radius measured from the center of the planet of 71,335 km. The density-altitude profiles of these three models are shown in figure 10.

For a probe to enter a massive planet like Jupiter, the inertial velocity is always nearly equal to the escape velocity. The nominal hyperbolic excess speed at Jupiter arrival is about 9 km/sec. The inertial entry speed is thus about 61 km/sec. If the entry is made in an equatorial posigrade direction, the entry speed relative to the rotating atmosphere can be reduced by about 12 km/sec due to the high rotation rate of Jupiter.

Typical altitude and relative velocity profiles for an eastward equatorial entry are shown in figure 11 for entry angles of -5°, -15°, -30°. A typical probe ballistic coefficient, m/C_DA, of 157 kg/m^2 was used. It should be noted that the probe goes subsonic at about 40 km above the cloud tops. The time of flight from the entry point of 305 km above the cloud top to this point is about 20 sec. It is therefore apparent that very large decelerations are incurred by the probe during entry. The maximum deceleration encountered as a function of entry angle is shown in figure 12 for entries into the model A, B, and C atmospheres. Decelerations in the thousands of Earth g are typical. Model C atmosphere has the lowest maximum acceleration because the high scale height of this model relative to models A and B.

After reaching subsonic speeds the heat shield of the probe will be discarded to eliminate the soak back of heat stored within the shield. About 2 minutes after entry the probe decelerates to a vertical terminal descent with a rate of sink of the order of 150 m/sec. The altitude at this time is about 30 km above the cloud tops. It is thus apparent that a rather long time is required to descend to pressures like 100 bars which occur at depths near 130 km below the cloud tops. The total descent time from the entry point (305 km above the cloud tops) to various atmospheric pressure levels is shown in figure 13 for all three atmospheric models discussed here. It can be seen that a descent time of the order 1 hour is required to reach 100 bars and that from 3 to 5 hours are required to reach 1000 bars. This descent time complicates the problem of maintaining communications between the probe and the flyby bus as will be discussed in a later section.

Entry thermal protection - A detailed discussion of the heat transfer and ablation material response characteristics for a Jupiter entry probe is beyond the scope and purpose of this report. References 16 and 17 contain such a discussion. Reference 17 presents the most recent and comprehensive parametric calculations of the environment and thermal protection requirements for such entries. The enthalpy and heating levels experienced by the entry probe are beyond current ability to experimentally verify all the extrapolations and assumptions used in that analysis. The analysis, however, is based on rather sound understanding of the possible phenomena. In summary, the analysis of reference 17 indicates that thermal protection system mass fractions of the order of 0.45 of the mass at entry are required to protect the probe during the deceleration to near sonic speed and that system weight is nearly constant (to the degree of uncertainty of the calculation) for

a wide range of entry angles, entry mass, and atmosphere composition. For the purposes of this analysis a constant value of thermal protection system mass fraction of 0.45 will be used.

Communications geometry— Communications between the entry probe and the flyby bus will be maintained by appropriate phasing of the entry and flyby trajectories to keep a line-of-sight between these two vehicles during the entire descent within given antenna constraints. In addition, atmospheric attenuation may be a severe problem so it is desirable to make the communications distance as small as possible. The primary problem in maintaining this geometry lies with the long time required during terminal descent to reach pressures of 100 bars and greater. As was shown earlier (fig. 13) descent times of the order of 45 minutes for the model B atmosphere are required to reach 100 bars and more than 4 hours are required to reach 1000 bars. Fortunately, the entry is nearly equatorial and posigrade so the rapid rotation of Jupiter about its axis (36°/hr) can be used to maintain line-of-sight for such long periods.

The problem of phasing between the entry probe and flyby bus involves the appropriate choice of periapsis altitude for the flyby trajectory and an appropriate phasing impulse at probe separation to either retard the probe or accelerate the bus. The geometry of the communications problem for the deflected bus mode is shown in figure 14(a). The slightly different geometry for the deflected probe mode is shown in figure 14(b). The mathematical development for the analysis of both modes is presented in appendix B. As shown in figures 14(a) and 14(b) the probe trajectory has four primary events: separation, entry, the beginning of terminal descent, and the time the design pressure is to be reached. Communication is to be maintained continuously (except for blackout) between separation and the time the design pressure is reached.

For this analysis, it was assumed that the antenna on board the bus was steerable and that the antenna on board the probe was isotropic over at least a 45° half-angle cone centered about the axis of the probe and looking aft. In addition, it was assumed that the entry probe was aerodynamically stable throughout entry and descent. The separation velocity requirements which meet the above antenna constraints between separation and 100 bars pressure for both the deflected bus and deflected probe modes are shown as a function of flyby periapsis radius for two separation positions in figures 15(a) and 15(b). Figure 15(a) presents results for an entry angle of -15° and figure 15(b) for an entry angle of -30°. It was found, as indicated by the shaded boundary to the left on each figure, that under these antenna constraints communication could not be maintained from the beginning of terminal descent to the 100 bar pressure level if the flyby bus periapsis radius was less than $1.5R_J$ and $1.25R_J$ for -15° and -30° entries, respectively. This boundary is caused by the high angular rate of the bus relative to the probe at lower periapsis radii which will not allow the required communication time of 45 minutes (see fig. 13). The shaded boundary on the right-hand side of figure 15(a) indicates the highest periapsis radius for which communication for the stated antenna constraints is possible both at entry and during terminal descent for a -15° entry. This boundary is caused by the low angular rate of the bus relative to the probe at higher periapsis radii which again will not allow a communications time of 45 minutes. The -30° entry (fig. 15(b)) is not limited communications considerations for high periapsis radius.

Since a low separation ΔV is desirable and since the separation accuracy for the deflected probe mode is enhanced for low periapsis radii (see fig. 8), flyby periapsis radii of $1.5R_J$ and $1.25R_J$ were chosen for -15° and -30° entries, respectively, along with a separation radius of $100R_J$.

The pertinent communications geometry parameters for the key events from the time of separation to the time the design depth of 100 bars is reached are shown in tables 5(a) and 5(b) for

-15° and -30° entries, respectively. The nominal model B atmosphere was assumed in both cases and results are shown for both the deflected bus and deflected probe modes. The parameters indicated are, first, the angle of the bus as seen from the probe relative to the probe antenna boresight. Positive angles indicate that the bus leads the probe. The next column indicates the angle that the bus antenna must swing to boresight on the probe for an inertially stabilized bus relative to the boresight position at the time the probe enters the atmosphere (i.e., event 2). Positive angles indicate that the bus antenna must slew in the aft direction. The next column indicates the relative communications distance between the probe and the bus. As mentioned before, the trajectories were picked to produce probe antenna look angles of less than ±45°. The bus antenna on an inertially stabilized vehicle must be capable of slewing at least 120° in order to track the probe to the 100 bar pressure level in the model B atmosphere. It should also be noted that the communication distance is maximum at the time of entry and is 65,000 and 86,000 km for the -15° and -30° entries, respectively.

Since the atmosphere structure will not be known prior to entry, it is appropriate to inquire about the effect on communications if the separation-phasing maneuver is made assuming the model B atmosphere exists but the model A or C atmosphere is actually encountered. The effect of atmosphere uncertainty upon the communications geometry problem is shown in tables 6(a) and 6(b) for -15° and -30° entries, respectively. In both tables results are presented for both model A and model C and for both the deflected bus and deflected probe modes. The major effects demonstrated by the results in these tables are (1) the communications problem if model A is encountered but is less stringent than the problem resulting from the planned encounter with model B, and (2) the longer descent times associated with the model C atmosphere results both in a probe-to-bus look angle greater than 45° and a much larger communication distance at the time that the design pressure is reached.

Entry targeting Targeting of the entry is, of course, primarily constrained by the location of the planetary features which are desirable objectives for entry missions as described previously. In addition, planetary approach conditions, the separation requirements for communications, and special requirements by certain instrumentation (e.g., solar lighting for the photometer experiment) further constrain the targeting problem.

The first probe should be targeted at the Equatorial Zone to sample cloud structure. The Equatorial Zone extends from about 7° S latitude to 7° N latitude. The results of the heliocentric trajectory analysis indicate that Type I trips of near 800 days and Type II trips of near 1200 days have nearly optimum characteristics. The approach conditions to Jupiter for the Type I and Type II trajectories are very different. The Type I transfer with a heliocentric transfer angle less than 180° arrives at Jupiter on the sunlit side. The Type II transfer with a heliocentric transfer angle greater than 180° arrives at Jupiter from outside its orbit. The separation and phasing requirements for communications between the probe and the bus dictate that the entry points for -15° and -30° entries must be about 135° and 110°, respectively, measured along a great circle from the approach asymptote. Finally, the requirements for sunlight for the photometer experiment during the descent to 100 bars requires, since that descent takes about 1 hour, that the entry be made at least 36° away from the eastward limb of the planet on the sunlit side. How these various factors constrain the targeting problem will now be discussed.

To illustrate the targeting problem, the stereographic meridional projection of planet surface is used. Since one of the prime constraints is solar lighting, the projection will for convenience be

centered upon the subsolar point at the time of arrival. The geometric visibility of various aspects of the targeting process achievable by this projection technique is very high. The primary advantage of this spherical projection is that all circles, great or minor, appear as circular arcs in the projection and the projection is isogonic, that is, inclination angles of planes relative to each other are preserved and can be measured with a protractor. A transparent orthogonal coordinate overlay allows for the graphical solution of all spherical geometric problems. The projection technique is described in appendix C.

Figures 16(a) to 16(d) contain the stereographic projections of Jupiter at the time of arrival for 800- and 1200-day trips during the 1978 and 1981 opportunities. The projections are centered upon the subsolar point at the time of arrival: thus, the outer edge of the hemispherical projection represents the terminator. Figure 16(a) shows the arrival conditions after an 800-day trip in 1978. At this time, the subsolar point lies slightly to the south of the equator and thus the south pole is seen in the projection. The -90° and -180° meridian lines in the inertial coordinate system of Jupiter are shown for reference. The latitude lines of 45° S and 45° N are also indicated. The tail of the arrival velocity vector relative to the planet is indicated by the crossed circle on the left side of the figure. The locus of entry points for the -15° and -30° entries are minor circles centered about the approach vector and are 135° and 110° great circle, respectively, away from the tail of the vector. They are indicated by the dash-dot lines so labeled. Finally, the region of the planet which is less than 1 hour from sunset is the region to the right of the dashed line. It can be seen that the -30° entry does satisfy the solar lighting constraint and that the -15° entry does not.

In figure 16(b), the darkside approach of the Type II 1200-day transfer during the same opportunity is shown. In this case, the head of the approach velocity vector is shown in the projection on the right side of the figure. Again the locus of possible entry points for the -15° and -30° entries is indicated by the labeled dash-dot lines. Since the approach is from the darkside, it is possible to satisfy the solar lighting constraint for a -15° entry for entries at latitudes from about 35° S to 45° N. In addition, the -30° trajectories enter nearly at the subsolar point for entries in the Equatorial Zone which may be advantageous for interpretation of the photometer data.

Figures 16(c) and 16(d) show almost identical conclusions for the Type I and Type II transfers, respectively, during the 1981 opportunity. Thus, in summary, at least a -30° entry angle is required for typical Type I transfers (of about 800 days duration) in order to obtain at least 1 hour of sunlight during the descent. For typical Type II transfers (of about 1200 days duration) entry angles slightly less than -15° may be used and still satisfy the solar lighting constraint. Equatorial entries near an entry angle of -30° have the advantage of nearly vertical solar lighting at entry and for some time during the descent.

An analysis has been made of the entry point dispersion based upon the guidance analysis previously presented. It has been determined that the 3σ dispersion ellipse at a -15° entry angle has a major axis along the trajectory plane 7.5° long (9300 km) and a minor axis normal to the trajectory plane approximately 1° wide (1250 km). The dispersion ellipse for a -30° entry is somewhat smaller. This dispersion does not appear to be serious considering the scale of the features to be hit.

ATMOSPHERE RECONSTRUCTION

The techniques for the reconstruction of atmosphere density structure from entry probe accelerometer, pressure, temperature, and spectrometer measurements are well documented and discussed in references 18 to 21. The techniques have been discussed primarily for the reconstruction of the atmospheres of Mars and Venus. Although the general technique is the same at Jupiter, some of the reconstruction accuracy problems are unique. This discussion will be on the general technique and some of the primary errors involved in the reconstruction of the Jovian atmosphere.

Reconstruction Technique

In summary, the atmosphere density profile is reconstructed from the measured acceleration profile as follows. The acceleration measured by the on-board accelerometers is the result of exterior forces. If the lift on the probe is zero, then the measured acceleration is simply the ratio of drag to mass and the density at some time τ in the trajectory after entry is determined from

$$\rho(\tau) = 2(m/C_D A)\left\{a(\tau)/[V(\tau)]^2\right\} \tag{1}$$

where $m/C_D A$ is the known ballistic parameter for the probe and $a(\tau)$ is the instantaneous acceleration. The instantaneous velocity $V(\tau)$ is determined from the equation of motion by integrating the accelerometer measurements from the known entry speed, V_E

$$V(\tau) = V_E - \int_0^\tau a\ dt - \int_0^\tau g\ \sin\gamma\ dt \tag{2}$$

The altitude corresponding to that instant in time and to the density calculated from equation (1) is found by integrating the vertical component of velocity from some reference altitude. For reasons to be discussed later that level shall be taken as the entry altitude.

$$h(\tau) = h_E + \int_0^\tau V \sin\gamma\ dt \tag{3}$$

The instantaneous flight-path angle γ is required in both equations (2) and (3) and can be determined from the solution of the differential equation of motion normal to the flight path.

$$d\gamma/dt = (V/r) - (g/V)\cos\gamma \tag{4}$$

where

$$r = R_J + h$$

The initial condition required for this solution is the known entry angle, γ_E

$$\gamma(0) = \gamma_E$$

It should be noted that the initial conditions V_E and γ_E are relative conditions measured relative to the rotating atmosphere.

The ballistic parameter m/C_DA which appears in equation (1) varies significantly with time because of the massive ablation mass loss of the heat shield. The results of reference 17 indicate that mass losses of the order of 30 percent of the entry mass can be expected during the deceleration to subsonic speeds. Thus, in order to complete the reconstruction analysis, a differential equation expressing the mass loss rate as a function of the instantaneous free-stream density and velocity must be solved with equations (1) to (4).

$$dm/dt = -f(\rho,V) \tag{5}$$

The initial condition is, of course, the known entry mass, m_E.

In principle, this technique should provide a perfect reconstruction (within the limits of the assumptions) if the measurement information is perfect. However, numerical integration errors accumulate and accelerometer systematic bias errors result in significant errors in the calculation of instantaneous velocity (eq. (2)) when the velocity is low relative to the entry speed. An error in velocity results in an error in density, altitude, and flight-path angle; thus a different technique must be used in this velocity regime.

After the probe is subsonic, it is possible to deploy instruments to measure static pressure and temperature. In addition, velocity might be measured directly with a pitot-static probe. If one is not available, however, velocity can be determined from the accelerometer by measuring the mean molecular weight of the atmosphere and then determining density directly from the pressure and temperature measurements. Then the accelerometer measurements, which are still accurate, are used to determine velocity from equation (1)

$$V(\tau) = \left\{ 2(m/C_DA)_S \, [a(\tau)/\rho(\tau)] \right\}^{1/2} \tag{6}$$

where $(m/C_DA)_S$ is the subsonic ballistic parameter. Equations (3) and (4) are used to determine the altitude and flight-path angle as before.

Obviously, the reconstruction hinges completely on the ability to establish the initial conditions of velocity and flight-path angle at entry and on the reference altitude. There is no particular problem in establishing the entry velocity to a sufficient accuracy and the entry angle is known to the uncertainty in guidance discussed in the previous section. The reference altitude, however, presents a unique problem.

Entry Altitude Errors

For entry probe missions to Mars and Venus, the time of impact with the surface is known and thus the impact can be used as an altitude reference. The atmosphere is then reconstructed from the bottom up. This is not possible at Jupiter. A similar difficulty arose in the interpretation

of the Russian Venera probe data at Venus. Since the probe failed before impact a reference altitude could not be established. The American Mariner occultation data of Venus, however, provided an upper atmosphere density reference which allowed the Russian data to be properly interpreted.

An occultation experiment has been included on the bus to provide the required high altitude reference for the interpretation of the probe data. This reference altitude will have an error associated with it which should be about the same order as the error in the reconstruction from tracking data of the flyby trajectory relative to Jupiter. Current evidence (e.g., see refs. 10 and 22) indicates that the flyby trajectory relative to Jupiter can be reconstructed to within 10 km from DSN (Deep Space Network) range and range rate data.

In addition to the occultation experiment, a photometer on the probe may be able to determine when the probe passes through the cloud layer and this level may be used as a reference. However, the cloud tops are highly irregular and the radius of the cloud tops is not known astronomically to within 350 km. Earlier flyby missions will probably reduce this uncertainty to about 50 km but the irregularities are still likely to be ±30 km.

Another alternative to determine a reference altitude is to measure the range from the probe to the bus. This would be accomplished by simply putting a transponder on the probe and measuring the two-way transmission time of a radio signal sent from the bus. If time can be measured to an accuracy of microseconds on the bus, then the probe trajectory relative to the bus can be reconstructed to an accuracy somewhat greater than the accuracy of the bus trajectory relative to Jupiter. Thus the radius of the probe at an acceleration of, say, 0.1g can be measured directly to within 10 km.

Entry Angle Errors

As mentioned before, the accuracy of the reconstruction of the atmosphere depends strongly on the accuracy within which the initial entry angle γ_E is known. As was also shown, the 3σ separation uncertainty in the entry angle for the deflected bus mode is about ±1.5°. The 3σ errors associated with the deflected probe mode are of the same order, being about ±2° at a -15° entry angle and about ±1.5° at a -30° entry angle (see fig. 8).

The errors in the reconstruction due to these entry angle errors were determined by using the computed acceleration profiles for entries into the nominal model B atmosphere across the range of uncertainty in entry angle. These profiles were then processed through the differential and integral equations of the previous section to produce atmosphere models. In each case the mean value for the entry angle was used as an initial condition for equation (4). In all cases the acceleration measurements were considered perfect. Measurement inaccuracies will be examined in the next section.

Figure 17(a) shows the uncertainty in the altitude-density profile for the 3σ uncertainty in entry angle of 2° about -15° for an entry using the deflected probe mode (nearly the same error as for the deflected bus mode). Also shown by the dashed line is the model B profile from which the acceleration profiles were calculated. It can be seen that even with exact knowledge of the entry angle, numerical errors accumulate and result in a 4-km error in the reconstruction of altitude at

densities near the cloud tops. It is also apparent that errors in the knowledge of the entry angle of $\pm 2^\circ$ result in an uncertainty in altitude at a given density of about ± 35 km near the cloud tops. The small discontinuities at about a density of 10^{-1} kg/m^3 are caused by the change at a Mach number of 0.8 from the set of equations used for the hypersonic and supersonic portion of the flight to those used during the subsonic portion.

If the entry angle is steeper, the effect of uncertainties in entry angle is considerably reduced. In addition, as was shown in the section on entry guidance, the uncertainty in entry angle is also reduced for steeper entries. Thus the guidance errors at -30°, for example, are less than $\pm 1.5^\circ$. The effect of this error on the atmosphere reconstruction at that entry angle is shown in figure 17(b). Altitude uncertainties of less than ± 15 km are apparent.

It is apparent from the results just presented that highly accurate knowledge of the entry angle is required for an accurate reconstruction of the atmosphere. In this regard both the deflected bus mode and the deflected probe mode are about equal. However, the alternative of ranging the probe from the bus was examined and it was determined that if time on board the bus could be measured to an accuracy of milliseconds, the entry angle of the probe for either trajectory mode could be determined from postflight data to an uncertainty of about $\pm 1/2^\circ$ (3σ). In this case, altitude uncertainties at a given density of the order of ± 10 km result from entry angle uncertainties alone. The entry angle of the probe for the deflected probe mode could be determined from postflight data to the same uncertainty as that for the deflected bus mode. In any case, altitude uncertainties at a given density of the order of ± 15 km have to be accepted from entry angle uncertainties alone.

Accelerometer Errors

Because it does not seem possible to calibrate the accelerometers to the high level of acceleration encountered during atmospheric entry (of the order of 1000g or more), systematic bias errors will be present in the accelerometer measurements. These errors will obviously affect the accuracy of the atmosphere reconstruction.

As an example of this effect, calculations have been made of the reconstruction of the model B atmosphere based upon the acceleration profile for a -15° entry with perfect knowledge of the entry angle and with a ± 1 percent bias on the accelerometer measurements. The resulting altitude-density profiles are presented in figure 18(a). A similar example is shown in figure 18(b) for a -30° entry. The reconstructed profiles deviate significantly from the model B profile at about 40-50 km above the cloud tops. In the subsonic flight regime (i.e., in the region below the discontinuity in the profiles) accelerometer bias errors do not seem to propagate, indicating that the primary error is in the reconstruction of velocity during supersonic flight (and its effect on the calculation of density) and only secondary in the reconstruction of altitude. A bias error of 1 percent results in an uncertainty in altitude at a given density of about 6 km at altitudes near the cloud tops.

Summary

There are, of course, other uncertainties associated with the reconstruction of the atmosphere. Primary among these is the uncertainty in ballistic parameter m/C_DA. The drag

coefficient C_D will not be known to high accuracy, and how it changes with Mach number and Reynolds number will be uncertain. A major problem will be the prediction of mass throughout the trajectory. Heat-shield ablation will cause the mass to change by 30 percent during the hypersonic portion of the entry (ref. 17). Knowledge of the way the mass ablates as a function of velocity and density is essential to a reasonably accurate reconstruction. Analysis of these effects is beyond the scope of this report but must be considered by more detailed studies.

The effects of uncertainties in the reference altitude and entry angle along with the effects of systematic accelerometer bias errors and the accumulation of numerical errors upon the atmospheric reconstruction amounts to a total uncertainty in altitude at a given density of at least ±15 km when these errors are root-sum-squared. This error is of the same order as the scale height of the postulated model B atmosphere.

These uncertainties are predicted upon range tracking the probe from the bus. A more detailed analysis is required to verify these results and to determine if ranging from the bus to the probe can be used below the entry level.

SYSTEMS ANALYSIS

This section is an analysis of the system options, requirements, and approximate weights of the entry probe and flyby bus. These vehicles satisfy, as much as possible, the science requirements previously discussed and make use of the operational description in the last section. Options involved in selection of a launch vehicle will be considered here. For convenience, the systems analysis discussion of the probe is presented first followed by a similar discussion and description of the bus design.

Probe Design

Payload instrumentation and data acquisition– The suggested probe instruments, their key support requirements, and operating conditions are shown in table 1. The background for these experiments and their associated measurement requirements were discussed in the section "Science Requirements."

A data profile has been derived from the probe trajectory and is shown in figure 19. This profile is based on the stated instrument complement, the nominal model B atmosphere, a probe entry angle of -15° and an m/C_DA of 157 kg/m^2. The probe trajectory produces a peak deceleration in excess of 1000 g; consequently, the instruments and associated circuitry must be hardened sufficiently to withstand the forces involved. The data acquisition profile is not really different for the -30° entry but the instruments and circuitry must be hardened for decelerations in excess of 2000 g.

During deceleration, communications blackout makes it necessary to store data for later transmissions. The estimated blackout region and the data storage requirement during this period are shown in figure 19. Following blackout the stored data are transmitted together with the real-time science at a fixed rate until the end of the mission.

During the passage through the postulated Jupiter trapped radiation belts, it is necessary to provide sufficient protection to make sure the electronic circuitry and components receive a dose of less than 10^4 rads. The photometer and other sensitive components should not be subjected to more than 10^3 rads. Calculation of the accrued dose at the outer edge of the heat shield of the probe using the postulated belt models of reference 23 indicates a dose of less than 10^4 rads. The added protection of the heat-shield material, supporting structure, and finally the structure of the pressure tight vessel for the descent to 100 bars is more than enough to reduce the accumulated dose of the instruments by more than an order of magnitude.

Data handling and communications– After separation from the bus, the probe will be spun up by an external cold gas system for stabilization during transit to the planet. The transmitter will be operable at a low power level (~2 W) to permit the probe to be tracked by the bus. Full transmitter and instrument power will be delayed until just prior to entry to conserve battery power. The tracking bandwidth will be increased from 50 to 200 Hz at the same time. This increase could be initiated either by a timer or by command from the bus should the timer fail or should higher power be needed momentarily, such as for reacquisition if probe tracking were interrupted.

Scientific data, including accelerometer readings in three orthogonal axes will be digitized, multiplexed, and encoded as shown in figure 20. The data stream will pass to a buffer and to the transmitter. The buffer will accumulate data only through the blackout period. After the high deceleration phase, as monitored by the accelerometers, the blackout data will be retransmitted by multiplexing with the ongoing scientific data.

A data rate of 100 bits/sec was selected as adequate to accommodate possible peak data loads including blackout data and some probe housekeeping or status telemetry. Any higher rate of data generation which might be required could easily be accommodated by increasing the capacity of the data storage unit already aboard the probe and transmitting the additional data later in the descent. The transmitter was sized on this basis, with emphasis on simplicity and low weight.

A transmitter frequency in the band between 100 and 5000 MHz is advisable to avoid the high noise emission of Jupiter. Furthermore, a frequency above 300 MHz is thought to be necessary to insure negligible refraction of the radio waves. In order to focus on the operating frequency, the computed performance margins were compared as a function of frequency as shown in figure 21. Both wide-band FSK (frequency shift keying) and narrow-band (frequency tracking) FSK are depicted as well as the effect of the diameter of the bus tracking antenna for a fixed beam width. Atmospheric attenuation was not considered in the calculation of this communications margin. Atmospheric attenuation will be considered in greater detail later in the discussion. This figure indicates that a frequency in the range of 500 to 1500 MHz would be optimum assuming a shroud constrains the antenna size to, say, 3 m. In addition, the margin available with the wide-band FSK system is not sufficient to overcome atmospheric attenuation which may run to 6 dB or more. A review of the elements of the link calculation for the narrow-band system that will highlight the necessary assumptions and design choices available is presented below.

Details of the elements of the probe-to-bus link calculation appear in table 7 for the narrow-band FSK system operating at a frequency of 800 MHz. First, a maximum transmitter power of 100 W was selected since it was felt that higher power would excessively burden the power supply and heat rejection systems of the probe. Solid-state transmitters of adequate efficiency and power should be available by the late 1970's over the frequency range under consideration. The

advantage of solid state is primarily its low voltage power supply requirements and low weight as compared to microwave tube devices that would be considered for higher power levels and frequencies. The ruggedness and reliability of solid state and traveling wave tubes, for example, is about comparable.

A probe antenna with nearly hemispherical coverage was assumed (uniform gain over ±45° of boresight is typical). Because of the relative angular displacement of the probe and bus, a probe tracking antenna on the bus was necessary. Tables 5 to 6(b) show that the angular motion of probe relative to the inertially stabilized bus between entry (event 2) and the beginning of terminal descent (event 3) is in the worst case 1.5°. Blackout occurs between these two events and it would be highly desirable if the bus antenna would not have to reorient its direction to reacquire the probe after blackout. Thus an antenna beamwidth with a 0.5 dB loss at 1.7° off the centerline was chosen to be conservative. This results in a half-power beamwidth of 8.5°. Only a modest gain (25.6 dB) antenna was possible within the tentative shroud constraint of 3 m.

A 3 dB loss was included for circuit losses, and the free space loss was estimated for the maximum communications distance (86,000 km for the -30° entry, see table 6(a)) resulting from the three atmosphere models assumed. Entry at -15° resulted in a rather small decrease in maximum communications distance down to 65,000 km. This results in a gain in communications margin of approximately 2.4 dB. It should be noted that for the -15° and -30° entries this maximum communication distance occurs at entry and that the communications distance decreases for entries into the nominal atmosphere when design pressure is reached. The distance at the design pressure is about 49,000 km and 25,000 km for the -15° and -30° entries, respectively. These distances produce a significant gain of 4.5 dB for the -15° entry and 10.7 dB for the -30° entry, above the margin shown in table 7. It must be remembered, however, that atmospheric attenuation has not been taken into account.

The main contribution to system noise temperature is the planetary disk which, at 800 MHz, is about 9100° K. A low noise (3.1 dB) traveling wave tube receiver is assumed aboard the bus. The result is a system noise temperature of 6460° K. The tracking FSK receiver must track over the bandwidth determined by oscillator instability of one part per million, a variation in the doppler shift due to a range of relative velocities up to 10 km/sec, and a signaling rate of 100 bits/sec. The signal-to-noise ratio required is that appropriate to narrow-band FSK for a bit error probability of 10^{-3}.

Going to a narrow-band system limits the amount of improvement since power must be allocated to the tracking circuits, which reduces that available for data transmission. The more narrow the tracking bandwidth the less power is required, but the time required for acquisition is increased and the tracking rate is reduced. The system is designed so that a change in frequency of 200 Hz/sec can be tracked, resulting primarily from a rate of change in range rate of 75 m/sec. The range rates during transit and during atmospheric descent after blackout are relatively stable; thus, the primary need for increased tracking capability is near blackout. The above capability results in an acquisition time of 2 seconds.

The primary source of attenuation may lie in the extreme pressure broadening of the ammonia absorption line. There are no data on the extent of broadening that might occur for small amounts of ammonia in high pressure mixtures of hydrogen. Unpublished estimates indicate that the total attenuation may run into the tens of decibels; thus every bit of margin that can be obtained should

be obtained. In this regard it appears that the -30° entry may have a distinct advantage over the -15° entry.

Configuration– During the hypersonic portion of the entry, gasdynamic heating, both radiative and convective, to a large extent dictates the configuration of the probe. In order to provide adequate aerodynamic stability and to minimize the thermal protection system weight (see ref. 17) a conical forebody configuration having a 60° half-angle was used in the weight estimate. A nearly hemispherical afterbody with RF transparent ablation material was used to complete the entry configuration.

After the probe has slowed to subsonic speeds, the thermal protection system is jettisoned and the configuration of the terminal descent package is spherical to resist the crush stress of the high pressures to be encountered. A forward location of the center of gravity would provide stability. Small auxiliary stabilizing surfaces may be required to keep the ball from tumbling. Pressure and temperature instrumentation is deployed outside the sphere. It has been estimated that the volume required within the descent sphere is about 0.056 m^3 (2 ft^3). Thus the diameter of the sphere is 0.48 m (19 in.).

In order to contain the spherical descent body and provide reasonable stability the center of gravity of the spherical descent body must be somewhat forward of two-thirds of the height of the forebody cone. Therefore, the base radius of the cone must be approximately 0.76 m (30 in.).

Weight estimate – A very preliminary estimate has been made of the weight of the probe based upon the science, communications, power, structures, and heat-shield requirements previously discussed and the elements of that weight are listed in table 8. The total weight of the spherical descent body is seen to be approximately 100 kg. Adding both forebody and afterbody heat shield and support structure makes the entry weight 242 kg. Adding then the spin-up motor and gas which is discarded prior to entry makes the probe weight at separation for the deflected bus mode 246 kg. The deflection maneuver for the deflected probe mode requires about 170 m/sec for both the -15° and -30° entries and thus requires a propulsion package of about 46 kg. The total weight of the probe system for the deflected probe mode is 292 kg. It should also be noted that the total power requirement for the probe is about 355 W.

Bus Design

Payload instrumentation and data acquisition – The suggested bus instruments, their key support requirements, and operating conditions are shown in table 2. The background for these experiments, how they support the entry experiments, and their associated measurement requirements were discussed in the section "Science Requirements."

A data profile for the flyby bus trajectory is shown in figure 22. The profile is based upon the instrument complement indicated in table 2 and a flyby periapsis radius of 1.5R_J which is associated with a -15° entry. The profile for the flyby periapsis radius of 1.25R_J associated with a -30° entry is only slightly different.

As was the case with the probe the instrumentation aboard the bus must be limited in accrued radiation dose to less than 10^4 rads. The vidicon, photometer, and other sensitive elements will

probably require additional protection to reduce the received dose to less than 10^3 rads. Again calculations of the accumulated dose during the entire planetary encounter indicate that it is of the order of 10^4 rads. Therefore localized protection is required for the more sensitive components.

Data handling and communications Data handling aboard the bus should present no unusual problems. Data from the probe, bus science and housekeeping data would be multiplexed and converted to a digital stream for transmission to Earth. During the Earth occultation phase, the total encounter data would be recorded simultaneously with its transmission to Earth. The reliability of the data is thus assured should components suffer degradation, making a lower data rate necessary, and permits repeated transmissions to determine transmission errors.

The bus-to-Earth communications link will employ conventional deep space techniques. A traveling wave tube transmitter aboard the bus will feed a large parabolic reflector. Modulation will be convolutionally coded PCM with subcarrier phase modulated on a 2300 MHz carrier. The receiver will be the 64 m (210 ft) antenna at Goldstone, California, and other similar stations if available. Table 9 summarizes the link parameters. A spacecraft effective radiated power (ERP) of greater than 32.8 dB is required to assure satisfactory carrier tracking. For the stated parameters, any desired data rate may be obtained with sufficient ERP aboard the spacecraft and consequent increases in spacecraft weight commensurate with the increase in ERP. A determination of the data rate must therefore include not only the scientific requirements and communications capability but must encompass the effects on spacecraft weight and mission reliability as well. The implications of this approach are investigated in the following section.

Weight estimate - In order to demonstrate the feasibility of the entry-probe mission to Jupiter it is necessary to at least estimate the approximate weight of the spacecraft to determine compatibility with available launch vehicles. To accomplish this, a computer program was used to synthesize unmanned spacecraft. The level of detail was sufficient to pinpoint the effects of specific configurational, operational, and state-of-the-art changes and limitations. This program incorporated the basic parameters needed to specify a spacecraft; the knowledge of these parameters is necessary to avoid specifying conflicting mission requirements.

The program was limited to unmanned spacecraft consisting of a science payload, communications, and supporting subsystems. The objective was to size elements of scientific spacecraft, as opposed to technology or applications satellites, and to omit any elements unique to a particular mission. Thus, the weight of shrouds, adapters, probes and landers must be determined independently of the program, and their weight added where necessary to that of the spacecraft. There is provision, however, to incorporate the impact of these unique elements, in terms of their weight and power load, on the spacecraft sizing. The scientific payload was similarly not specified and its influence on the program is by means of its weight, power, data storage and attitude stabilization accuracy requirements, and ultimately by the data rate needed to telemeter the scientific measurements to Earth.

The weight of the flyby spacecraft has been estimated by means of a spacecraft sizing computer program, based on the science requirements, a midcourse maneuver requirement of 40 m/sec prior to separation, a trip time of 1200 days, and a communications distance of 5.6 a.u. Spacecraft were sized for both the baseline science package of 47 kg and a more inclusive science package of 97 kg as described in table 2. The science payloads include relay radio and data handling equipment and a scan platform. An allowance of 27 kg was provided for a 3 m probe tracking antenna and 16 kg for probe mounting hardware.

The propulsion subsystem was based on a motor having an inert mass fraction of 1.2 and an I_{sp} of 235 seconds. Power was supplied by boom-mounted RTGs.

Figure 23 shows the resulting spacecraft weight for the deflected probe mode (excluding the probe) as a function of data rate to Earth for the baseline and complete science packages. The solid curves indicate the minimum weight vehicle for each data rate. At each data rate there exists a different combination of antenna diameter and transmitter power for a minimum weight system. For example, at 10,000 bits/sec, a 6 m dish and 33 W transmitter is required to achieve minimum weight. If a shroud constrains the antenna to 3 m, the transmitter power rises to 107 W to meet the data rate requirement, and the spacecraft weight is increased as shown by the dotted curve. The spacecraft weight for the deflected bus mode is larger by the weight of the deflection propulsion system and the associated increase in weight of the structure and attitude control system.

Three data rates are indicated on figure 23. With the lower rate (800 bits/sec) it is possible to transmit all nonimaging data in real time. However, at encounter, imaging and other science data would have to be recorded and transmitted after the flyby was completed. This has an obvious disadvantage in that most of the data is transmitted only after two passages through the radiation belts, and mission success is dependent upon the successful operation of a tape recorder.

If weight permits, a higher data rate makes it possible to transmit the imaging data as acquired. A rate of 8500 bits/sec is required for the baseline science or 9000 bits/sec is required for the complete science package.

A summary of estimated subsystem weights is given in table 10 for the deflected probe mode, for the baseline and complete science packages, and for both the nonreal and the real time transmission of the data. An antenna constraint of 3 m was employed. A redundant 3×10^8 bit recorder is employed, regardless of the operational mode, to increase probability of mission success, and since some tape recorder capacity (about 3×10^6 bits) is necessary anyway for the 1.5 hours of Earth occultation. Spacecraft weights excluding the probe are seen to range from about 550 to 1000 kg.

Similar results are shown in table 11 for the deflected bus mode. Here because of the increased propulsion requirements to deflect the bus, the spacecraft weight excluding the probe ranges from about 700 to 1200 kg.

Total System Weight

Tables 10 and 11 show that the total system weight is the sum of the appropriate probe weight and bus weight for both the deflected probe and deflected bus mode. For the deflected probe mode, the total system weight, depending on the weight of the science package on board the bus and the data rate back to Earth, ranges from 830 to 1270 kg. The weights for the deflected bus mode are about 100 to 200 kg heavier because the propulsion system for deflecting the bus is heavier than that for deflecting the probe. The range of weights for the deflected bus mode is 920 to 1440 kg.

Launch Vehicle Selection

Six launch vehicle combinations have been examined as possible candidates for this mission. The selected launch vehicles are:

1. Atlas/Centaur/Burner II
2. Saturn 1B/Service Module/Burner II
3. Titan IIID (5 segment)/Centaur
4. Titan IIID (5 segment)/Centaur/Burner II
5. Titan IIID (7 segment)/Centaur
6. Titan IIID (7 segment)/Centaur/Burner II

Payloads for these vehicles as a function of the mission characteristic velocity are shown in figure 24. The characteristic velocity (V_C) for a mission is the sum of the incremental velocity requirement from Earth parking orbit and the propulsive velocity necessary to achieve the nominal 185 km parking orbit (about 7.8 km/sec). A V_C range of 14.1 to 15.2 km/sec is typical of the lower energy Jupiter flyby missions in figures 1(a) and 1(b).

The first vehicle, the Atlas/Centaur/Burner II, has a capability to boost a 100 to 300 kg spacecraft on a Jupiter flyby. This is far below the requirement derived by this analysis. The Saturn 1B/Service Module/Burner II has a maximum payload capability for this mission of about 590 kg. This is also too low. It can be seen from figure 24 that of those considered only the Titan family of launch vehicles has the capability to launch payloads greater than 1000 kg. It should also be noted that including the Burner II stage on top of the stack only adds to the payload of the Titan/Centaur combinations at higher characteristic velocity requirements.

Comparing the capability of the Titan/Centaur vehicles with the total payload requirements given in tables 10 and 11 and the velocity requirements including a 20-day launch window (figs. 1(a) and 1(b)) leads to the following conclusions. First, the five-segment Titan IIID/Centaur can be used to launch a spacecraft using either the deflected bus mode or the deflected probe mode with a margin of about 25 percent provided that nonreal time transmission of the imaging data is used (i.e., the bit rate is of the order of 800 bits/sec). The Burner II upper stage may be required to provide a 20-day launch window for the 1978 and similar opportunities. Finally, the seven-segment Titan IIID/Centaur is required to launch a spacecraft using either the deflected bus mode or the deflected probe mode with a margin of about 25 percent for the favorable 1981 opportunity if real-time transmission of the imaging data is required (i.e., with a bit rate of the order of 9000 bits/sec) and if the antenna is constrained to 3 m in diameter. The more difficult 1978 opportunity velocity requirement can be met for the larger payload with this booster but with very little margin. The addition of the Burner II upper stage does not in this case have any significant effect in opening the launch window.

NOMINAL MISSION DESCRIPTION

A preliminary analysis of the most important aspects and the feasibility of conducting an atmosphere-entry probe mission to Jupiter has been presented in the previous sections. The most

important conclusions of that analysis are presented in the section "Summary and Conclusions." A concise description of the suggested mission is presented below.

The basic scientific purpose of the mission is to increase understanding of the origin and evolution of the solar system and to investigate the possibilities of finding the beginnings of life on the Jovian planets. To help accomplish these broad goals, the atmospheric probe would obtain data on the structure and composition of the atmosphere and would conduct some chemical analyses. The target entry point for the probe would be in the equatorial zone of Jupiter within a very few degrees of latitude of the equator.

The probe would be carried and supported on the way to Jupiter by an interplanetary three-axis stabilized spacecraft. The spacecraft probe combination could be launched upon a five-segment Titan IIID/Centaur/Burner II launch vehicle combination or by the Shuttle during the early 1980's. After a trip time of about 1200 days, the spacecraft and probe would arrive at the near vicinity of Jupiter. The spacecraft would be targeted for a posigrade equatorial flyby with a radius of closest approach of about 89,000 km. At a distance from Jupiter of about 7×10^6 km the probe would be separated and deflected toward the planet and targeted for an inertial entry angle of about -30°.

After experiencing a deceleration of about 2000 Earth g and immense gasdynamic heating, the probe slows to subsonic speeds and begins its terminal descent into the atmosphere. The thermal protection system is jettisoned and the spherical descent ball of instrumentation descends for about 45 minutes until it reaches the design pressure of 100 bars. During the terminal descent, data are telemetered to the flyby bus which is within line of sight.

In addition to the data obtained by the probe, complementary data would be obtained remotely by the flyby bus. These data would be primarily in the form of moderate resolution images of the entry point and atmospheric occultation of spacecraft radio signals. This information and the probe data could be stored and replayed at a moderate data rate to Earth after the planetary encounter.

National Aeronautics and Space Administration
Moffett Field, Calif., July 8, 1971

APPENDIX A

SEPARATION ANALYSIS FOR THE DEFLECTED PROBE MODE

The analysis of the separation problem for entry from a flyby trajectory using the deflected probe mode is based upon the geometry shown in figure 7. The two primary sources of error (an error in the magnitude and an error in the direction of application of the deflection impulse) are treated below.

ERROR IN DEFLECTION IMPULSE MAGNITUDE

To determine the entry angle error due to an error in the magnitude of the deflection velocity increment, the equation for conservation of angular momentum along the impacting trajectory

$$V_e r_e \cos \gamma_e = V_2 r_s \cos \gamma_2 \tag{A1}$$

is differentiated with respect to the flight-path angle γ_2 to yield

$$d\gamma_e/d\gamma_2 = \tan \gamma_2/\tan \gamma_e \tag{A2}$$

If the simplifying assumption is made that V_2 is about equal to V_1, the deflection velocity increment can then be approximated by

$$\Delta V \cong 2V_2 \sin (\Delta\gamma/2) \tag{A3}$$

Differentiating equation (A3) and noting that $d\,\Delta\gamma = d\gamma_2$ and substituting into equation (A2) yields the following equation for the error in the entry angle due to an error in the magnitude of ΔV.

$$d\gamma_e = 2 \tan(\Delta\gamma/2)(\tan \gamma_2/\tan \gamma_e)(d\,\Delta V/\Delta V) \tag{A4}$$

ERROR IN DEFLECTION IMPULSE DIRECTION

To determine the entry angle error due to an error in the direction of the deflection velocity increment, equation (A1) is now differentiated with respect to the velocity V_2 to yield

$$d\gamma_e/dV_2 = [r_e \cos \gamma_e(dV_e/dV_2) - r_s \cos \gamma_2]/(r_e V_e \sin \gamma_e) \tag{A5}$$

From the conservation of energy equation

$$dV_e/dV_2 = V_2/V_e$$

In addition, the error in V_2 caused by an error in the direction of application of the deflection velocity increment is

$$dV_2 = \Delta V \, d\theta$$

where $d\theta$ is the error in the application angle and ΔV is determined from equation (A3). Substituting the above equations into equation (A5) and using equation (A1) yields the equation for the error in the entry angle due to an error in the direction of ΔV

$$d\gamma_e = 2[(V_2^2 - V_e^2)/V_e^2] \, [\sin(\Delta\gamma/2)d\theta/\tan\gamma_e] \qquad \text{(A6)}$$

APPENDIX B

COMMUNICATIONS GEOMETRY

The analysis of the communications problem between the probe and bus is for the deflected bus and the deflected probe modes based on the geometry shown in figures 14(a) and 14(b), respectively.

DEFLECTED BUS MODE

In the deflected bus mode the characteristics of the undisturbed impacting probe trajectory are determined from the given entry angle, γ_e, the entry radius, r_e, and the known hyperbolic excess speed, V_∞.

$$\tan \gamma_e = (e_p \sin \theta_e)/(1 + e_p \cos \theta_e) \tag{B1}$$

$$r_e = [a_p(1 - e_p^2)]/(1 + e_p \cos \theta_e) \tag{B2}$$

$$a_p = -\mu/V_\infty^2 \tag{B3}$$

If equations (B1), (B2), and (B3) are combined, the unknown eccentricity of the probe trajectory can be obtained as follows:

$$e_p = \left\{1 + [1 - (2a_p/r_e)]/[(a_p/r_e)^2 (\tan^2 \gamma_e + 1)]\right\}^{1/2}$$

The true anomaly of entry on the probe trajectory $\theta_{e,p}$ is then determined from

$$\cos \theta_{e,p} = [(a_p/r_e)(1 - e_p^2) - 1](1/e_p)$$

and

$$\sin \theta_{e,p} = -\sqrt{1 - \cos^2 \theta_{e,p}}$$

Similarly, the true anomaly of separation on the probe trajectory, $\theta_{s,p}$ is determined from the given separation radius, r_s, as

$$\cos \theta_{s,p} = [(a_p/r_s)(1 - e_p^2) - 1](1/e_p)$$

and

$$\sin \theta_{s,p} = -\sqrt{1 - \cos^2 \theta_{s,p}}$$

From the vector diagram in figure 14(a), the characteristics of the deflected bus trajectory can be determined if the periapsis radius, r_p, and the phasing velocity increment, V_p, are specified. The velocity of the bus after separation, V_2, is simply

$$V_2 = V_1 + V_p \tag{B4}$$

and

$$V_1^2 = \mu(2/r_S) + V_\infty^2 \tag{B5}$$

The conservation of energy yields

$$V_2^2 = \mu(2/r_S) - [(1 - e_B)/r_p]$$

or the eccentricity of the bus trajectory is

$$e_B = 1 - (2r_p/r_S) + (r_p V_2^2/\mu)$$

where V_2 is determined from equations (B4) and (B5) the true anomaly on the deflected bus trajectory at separation is then given by

$$\cos\theta_{s,B} = [(r_p/r_S)(1 + e_B) - 1](1/e_B)$$

and

$$\sin\theta_{s,B} = 1\sqrt{1 - \cos^2\theta_{s,B}}$$

The required separation velocity increment, ΔV, can now easily be obtained from the magnitudes of V_1 and V_2 and the difference in flight-path angle at separation.

$$\Delta V = [(V_2 - V_1 \cos\Delta\gamma)^2 + (V_1 \sin\Delta\gamma)^2]^{1/2}$$

where

$$\Delta\gamma = \gamma_{s,B} - \gamma_{s,p}$$

and

$$\tan\gamma_{s,B} = (e_B \sin\theta_{s,B})/(1 + e_B \cos\theta_{s,B})$$

$$\tan\gamma_{s,p} = (e_p \sin\theta_{s,p})/(1 + e_B \cos\theta_{s,p})$$

With the two trajectories completely specified the communication parameters such as range and antenna look angles are easily computed. The three free parameters, periapsis radius, r_p, separation radius r_S, and the phasing velocity increment V_p, are then systematically varied until suitable communication geometry is found.

DEFLECTED PROBE MODE

In the deflected probe mode the analysis is very similar except the undisturbed trajectory is that of the bus. Therefore the eccentricity of the bus trajectory for a given periapsis radius r_p is

$$e_B = 1 - (r_p/a_B)$$

where

$$a_B = -(\mu/V_\infty^2)$$

The true anomaly of the separation on the bus trajectory is obtained as before with the value of eccentricity and the given separation radius.

The semimajor axis of the deflected impacting probe trajectory is determined from the energy equation and the given value of the phasing increment, V_p (see fig. 14(b)). Thus,

$$V_2 = V_1 - V_p \tag{B6}$$

where

$$V_1^2 = \mu(2/r_S) + V_\infty^2 \tag{B7}$$

and

$$a_p = 1/[(2/r_S) - (V_2^2/\mu)] \tag{B8}$$

The characteristics of the probe trajectory can be calculated as in the deflected bus mode where equations (B6), (B7), and (B8) are used in place of equation (B3).

The calculation of the deflection velocity increment and the communication parameters is then identical to that for the deflected bus mode. Calculations have shown that, for practical purposes, the required velocity increment and the resulting communication parameters are identical for the same separation radius, periapsis radius, entry angle, and phasing velocity increment, as might be expected.

APPENDIX C

CONSTRUCTION OF THE STEREOGRAPHIC PROJECTION

The stereographic meridional projection has been known by cartographers for centuries. More recent analysis (ref. 24) indicated its use for the solution of a wide variety of three-dimensional problems and delineated the detailed steps necessary for point-by-point construction. The basic characteristics of the projection (i.e., all circles project as circles and all angles are preserved) make it of great use in orbit analysis.

Since one of the main constraints on the targeting of an entry probe at Jupiter involves the requirement for solar lighting during the entry mission, a projection about the subsolar point is convenient. This appendix describes the construction of such a subsolar point projection. It should be noted that the projection can be made about any point on the planet. Selection of the point is based on one of the primary requirements of the mission. Other examples of alternative projection points at other planets might be the sub-Earth point in a bistatic radar experiment, the arrival excess velocity vector for an orbiting mission (all orbits would be straight lines through the center of the projection), or a desired landing point.

In order to draw the projection, one needs a straightedge, a compass, and an orthogonal coordinate overlay as shown in figure 25. The overlay is merely a projection about a point on the equator of the planet. Thus, the longitude lines (meridians) are circles centered along the equatorial plane and the latitudes are circles centered along the polar axis. Both the meridians and the latitudes represent equal angular intervals. The construction of the overlay is shown in figure 26.

The first step in the development of the projection is to draw the great circle, which is 90° from the projection center (i.e., "primitive circle"), defining the hemisphere of interest. Then, the vertical and horizontal reference lines are drawn through the projection center (fig. 27). Next, the overlay is centered on the projection (fig. 27), and the equator, pole, and latitude lines desired are marked on the vertical reference. As an illustration, if a subsolar projection is desired where the declination of the subsolar point is 20° and the right ascension is 135°, then the equator arc would cross the vertical reference line 20° below the projection center. The North Pole would be 70° above the projection center and the vertical reference line becomes the 135° longitude line. Latitudes can then be ticked at the desired intervals along the vertical reference line. The equator can also be established since, being a great circle perpendicular to the polar plane containing the projection point, it intersects the "primitive circle" coincident with the horizontal reference line and since its angular distance from the projection center on the vertical reference line is known. It is, therefore, constructed in the same manner as the meridians of figure 26. It may also be drawn by positioning the vertical reference of the overlay over the horizontal reference of the projection and sketching the equator. With the overlay in this position, the desired longitudes may be marked along the equator.

The next step is to lay out the desired latitude and longitude lines. This is done by centering the overlay on the projection and then rotating the overlay until one of the meridian (interpolation may be required) lines intersects the vertical reference line at the North Pole and the equator at the desired longitude. The longitude lines can now be sketched by interpolation on the overlay. For greater accuracy, after the overlay is positioned as above, the poles can be marked on the primitive

circle and the perpendicular bisector drawn. The longitude line is an arc of a circle, centered on the perpendicular bisector, which passes through the poles (see fig. 28). The center of the circle is found by measuring the angle on the overlay grid from the projection center to the meridian which intersects the North Pole and the equatorial longitude desired. The construction is performed as for a meridian in figure 26. While the overlay is positioned for the longitude lines, the latitudes can be marked on the longitude line measuring from the North Pole. The lines of constant latitude will be arcs of circles centered along the vertical reference line and passing through the marks on the longitude lines. The compass is moved by trial and error until the proper center location is found so that the circle connects the desired points on the projection.

Once the projection grid is established, the known data points of interest can be plotted (e.g., arrival excess velocity vector, sub-Earth point, etc.) by use of their right ascensions and declinations. Desired reference planes (e.g., ecliptic plane) can also be shown. These data for a sample case (RA V_∞ = 220°, Decl V_∞ = 10°, $RA_\oplus$ = 112°, and $Decl_\oplus$ = 25°) are shown in figure 29.

Additional parametric data (i.e., multiple solutions for a fixed set of arrival conditions), such as solar lighting angle or entry positions, can also be shown on the projection by relating the data to the planet central angle.

REFERENCES

1. Anon.: Space Research: Directions for the Future: Report of a Study by the Space Science Board. National Research Council Publication 1403, 1966.

2. Anon.: The Outer Solar System – A Program for Exploration. Natl. Acad. Sci., June 1969.

3. Hadley, G.: Concerning the Cause of the General Trade Winds. Phil. Trans. Roy. Soc. London, vol. 39, no. 437, 1735, pp. 58-62. (Reprinted in Abbe, C.: The Mechanics of the Earth's Atmosphere. Third Collection. Smithsonian Miscellaneous Collections, vol. 51, no. 4, The Smithsonian Institution, 1910, pp. 5-7.)

4. Lewis, John S.: Observability of Spectroscopically Active Compounds in the Atmosphere of Jupiter. Icarus, vol. 10, no. 3, May 1969, pp. 393-409.

5. Westphal, J. A.: Observations of Localized 5-Micron Radiation From Jupiter. Astrophys. J., vol. 157, no. 1, pt. 2, July 1969, pp. L63-L64.

6. Gehrels, Thomas: The Transparency of Jovian Polar Zones. Icarus, vol. 10, no. 3, May 1969, pp. 410-411.

7. Gross, S. H.; and Rasool, S. I.: The Upper Atmosphere of Jupiter. Icarus, vol. 3, no. 4, Nov. 1964, pp. 311-322.

8. Taylor, D. J.: Spectrophotometry of Jupiter's 3400-10,000 Å Spectrum and a Bolometric Albedo for Jupiter. Icarus, vol. 4, no. 4, Sept. 1965, pp. 362-373.

9. Lewis Research Center: Performance Evaluation of Atlas-Centaur Restart Capability in Earth Orbit. NASA TM X-1647, 1968.

10. Anon.: Guidance and Navigation Requirements for Unmanned Flyby and Swingby Missions to the Outer Planets. Vols. I-III, Massachusetts Inst. Tech., Contract NAS2-5043, 1970.

11. Lewis, John S.: The Clouds of Jupiter and the NH_3-H_2O and NH_3-H_2S Systems. Icarus, vol. 10, no. 3, May 1969, pp. 365-378.

12. Hogan, Joseph S.: The Thermal Structure of the Jovian Atmosphere. J. Atmos. Sci., vol. 26, no. 5, pt. 1, Sept. 1969, pp. 898-905.

13. Barger, A. R.: Engineering Models for the Atmosphere of Jupiter. Martin Marietta, Denver Div., Internal Memo, June 1969.

14. Trafton, L. M.: Model Atmospheres of the Major Planets. Astrophysics J., vol. 147, no. 2, 1967, pp. 765-781.

15. Hunten, Donald M.: The Upper Atmosphere of Jupiter. J. Atmos. Sci., vol. 26, no. 5, pt. 1, Sept. 1969, pp. 826-834.

16. Tauber, M. E.: Atmospheric Entry Into Jupiter. J. Spacecraft Rockets, vol. 6, no. 10, Oct. 1969, pp. 1103-1109. (AIAA Paper 68-1150.)

17. Tauber, M. E.; and Wakefield, R. M.: Heating Environment and Protection During Jupiter Entry. AIAA Paper 70-1324, 1970.

18. Seiff, A.: Some Possibilities for Determining the Characteristics of the Atmospheres on Mars and Venus From Gas-Dynamic Behavior of a Probe Vehicle. NASA TN D-1770, 1963.

19. Seiff, Alvin; and Reese, David E.: Use of Entry Vehicle Responses to Define the Properties of the Mars Atmosphere. Proc. AAS Meeting on Unmanned Exploration of the Solar System, Denver, Colorado, Feb. 1965, pp. 419-445.

20. Peterson, V. L.: A Technique for Determining Planetary Atmosphere Structure From Measured Accelerations of an Entry Vehicle. NASA TN D-2669, 1965.

21. Seiff, Alvin: Direct Measurements of Planetary Atmospheres by Entry Probes. AAS Paper 68-187, 1968.

22. Rechtin, Eberhardt: Long-Range Planning for the Deep Space Network. Astronaut. Aeron., vol. 6, no. 1, Jan. 1968, pp. 28-35.

23. Meston, R. D.: Technological Requirements Common to Manned Planetary Missions Appendix B. Space Div., North American Rockwell Corp., Contract NAS2-3918, Jan. 1968.

24. Godet, S.: Solving 3-D Problems Made Simple by Stereographic Projection. Space/Aeronautics, vol. 33, no. 5, May 1960, pp. 59-65 and vol. 33, no. 6, June 1960, pp. 114-118.

TABLE 1.- JUPITER PROBE INSTRUMENTATION

Instrument	Minimum cycle time, sec	Bits/ cycle	Altitude regime, km	Resolution/ sample, km	Weight, kg	Required power, W
Accelerometers	10^{-3}	40	228 to -132	0.2 sec, 1 km*	3.2	4
Temperature	10^{-3}	8	50 to -132	1		.2
Pressure	10^{-3}	8	228 to -132	1		.1
Photometers	10^{-3}	40	50 to -132	1	1.0	1
Gas chromatograph/ mass spectrometer	120	600	50 to -132	10	3.2	12

Note: Total volume requirement of about 400 $in.^3$

*Samples at 0.2-sec intervals to 50-km altitude and at 1-km intervals to 100 bars

TABLE 2.– FLYBY BUS INSTRUMENTATION

Instrument	Spectral range, μ	Spectral resolution, μ	Spatial resolution, m	Bits/ sample	Maximum bit rate, bits/sec	Weight, kg	Required power, W
Baseline complement							
Optical imaging	0.4–0.7		1×10^4	10^6	8.3×10^3	5	10
IR radiometer	10–25		6.5×10^5	28	0.9	1.4	3
UV photometer	0.0584, 0.105–0.125		6.5×10^5	30	1	.5	3
Radio occultation				8	8	2.3	1.5
Particles*			2×10^4	64	64	11	8
Fields**			2×10^4	22	22	3.7	7
Additional desirable experiments							
IR spectrometer	1–20	10^{-4}	6.5×10^5	5×10^3	1.6×10^2	18	8
UV spectrometer	0.05–0.3	10^{-4}	6.5×10^5	10^4	3.3×10^2	16	13
Topside sounder†					10	3.7	10
Very low frequency‡				50	5	2.3	4

*Electrons > 40 keV and proton < 100 keV

**Field strengths of 1 γ – 10 gauss

†3–50 MHz

‡0.7–10 MHz

TABLE 3.– MINIMUM ENERGY HELIOCENTRIC TRAJECTORIES TO JUPITER – 1978 OPPOSITION

Trip time, days	400	600	800	1000	1200	1400	1600
Date leave Earth	3790	3790	3790	3800	3790	3800	3820
Date arrive Jupiter	4190	4390	4590	4800	4990	5200	5420
Characteristic velocity, km/sec	17.1	14.94	14.61	14.99	14.63	14.45	14.43
Leave Earth							
Right ascension	117.0	99.6	97.3	97.8	113.7	124.3	130.4
Declination	25.4	31.8	41.3	50.3	-.8	5.6	5.4
Arrive Jupiter							
Right ascension	335.6	354.3	346.0	334.0	327.3	328.9	336.4
Declination	-1.0	-2.1	-5.7	-9.9	5.5	2.8	2.8
Communications distance, a.u.	5.59	5.45	5.58	5.69	5.50	5.70	4.88

TABLE 4.– MINIMUM ENERGY HELIOCENTRIC TRAJECTORIES TO JUPITER – 1981 OPPOSITION

Trip time, days	400	610	710	810	1010	1200	1400
Date leave Earth	4980	4970	4970	4970	4970	4980	4990
Date arrive Jupiter	5380	5580	5680	5780	5980	6180	6390
Characteristic velocity, km/sec	16.92	14.65	14.31	14.15	14.10	14.15	14.27
Leave Earth							
Right ascension	202.7	193.8	191.5	192.2	199.9	209.2	221.3
Declination	-5.5	.1	1.4	1.4	-2.7	-1.5	-5.0
Arrive Jupiter							
Right ascension	86.7	85.0	81.5	76.0	63.5	58.3	61.7
Declination	3.2	3.0	3.0	5.8	2.9	1.4	1.3
Communications distance, a.u.	5.51	5.34	6.27	5.34	5.23	5.19	5.10

TABLE 5.— PROBE-TO-BUS COMMUNICATIONS PARAMETERS

Entry mode	Entry event	Time from separation, hr	Probe antenna look angle, deg	Bus antenna look angle, deg	Communications distance, km
(a) $\gamma_e = -15°$; $r_p = 1.5R_J$; $r_s = 100R_J$; $V_\infty = 9$ km/sec; model B atmosphere					
Deflected bus	Separation	0	---	-19.9	0
	Entry	149.68	30.5	0	64,900
	Terminal descent	149.71	-44.9	-1.5	63,500
	100 bars	150.46	44.6	-117.8	48,800
Deflected probe	Separation	0	---	-19.8	0
	Entry	150.26	30.4	0	65,100
	Terminal descent	150.29	-45.0	-1.4	63,600
	100 bars	151.04	44.4	-117.7	48,600
(b) $\gamma_e = -30°$; $r_p = 1.25R_J$; $r_s = 100R_J$; $V_\infty = 9$ km/sec; model B atmosphere					
Deflected bus	Separation	0	---	-33.7	0
	Entry	149.25	18.5	0	86,000
	Terminal descent	149.28	-42.9	-.4	84,200
	100 bars	150.03	44.9	-114.8	24,800
Deflected probe	Separation	0	---	-33.7	0
	Entry	149.49	18.5	0	86,000
	Terminal descent	149.52	-42.9	-.5	84,200
	100 bars	150.27	44.8	-115.0	24,900

TABLE 6. EFFECTS OF ATMOSPHERIC UNCERTAINTIES ON COMMUNICATIONS

(a) $\gamma_e = -15°$: $r_p = 1.5R_J$

Entry mode	Entry event	Time from separation, hr	Probe antenna look angle, deg	Bus antenna look angle, deg	Communications distance, km
Model A atmosphere					
Deflected bus	Separation	0	- - -	-19.9	0
	Entry	149.68	30.5	0	64,900
	Terminal descent	149.70	-45.1	-1.2	63,800
	100 bars	150.21	15.5	-72.3	36,700
Deflected probe	Separation	0	- - -	-19.8	0
	Entry	150.26	30.4	0	65,000
	Terminal descent	150.28	-45.2	-1.2	63,900
	100 bars	150.79	-8.9	-72.4	36,100
Model C atmosphere					
Deflected bus	Separation	0	- - -	-19.9	0
	Entry	149.68	30.5	0	64,900
	Terminal descent	149.71	-45.5	-1.4	63,500
	100 bars	150.79	59.5	-143.8	77,800
Deflected probe	Separation	0	- - -	-19.8	0
	Entry	150.26	30.4	0	65,000
	Terminal descent	150.29	-45.6	-1.4	63,600
	100 bars	151.37	59.4	-145.2	77,600

TABLE 6.– EFFECTS OF ATMOSPHERIC UNCERTAINTIES ON COMMUNICATIONS – Concluded

(b) $\gamma_e = -30°$; $r_p = 1.25R_J$

Entry mode	Entry event	Time from separation, hr	Probe antenna look angle, deg	Bus antenna look angle, deg	Communications distance, km
Model A atmosphere					
Deflected bus	Separation	0	---	-33.7	0
	Entry	149.25	18.5	0	86,000
	Terminal descent	149.27	-43.0	-.3	84,600
	100 bars	149.78	-21.7	-39.9	32,100
Deflected probe	Separation	0	---	-33.7	0
	Entry	149.49	18.5	0	86,000
	Terminal descent	149.51	-42.9	-.3	84,600
	100 bars	150.02	-21.6	-40.0	32,000
Model C atmosphere					
Deflected bus	Separation	0	---	-33.7	0
	Entry	149.25	18.5	0	86,000
	Terminal descent	149.28	-43.6	-.3	84,200
	100 bars	150.36	88.2	-170.8	59,700
Deflected probe	Separation	0	---	-33.7	0
	Entry	149.49	18.5	0	86,000
	Terminal descent	149.52	-43.6	-.3	84,200
	100 bars	150.60	88.2	-170.9	59,800

TABLE 7.– NARROW-BAND PROBE TO BUS RELAY LINK MARGIN AT 800 MHz

Transmitter, 100 W	20.0 dB	
Probe antenna gain	3.0	
Bus antenna gain, 3 m	25.6	
Bus antenna pointing loss	-0.5	
Total circuit loss	-3.0	
Free space loss, 86,000 km	-189.2	
Received power, P_r	-144.1	
Noise, N_O, T = 6460° K	-190.5	
Signal/noise received, P_r/N_O	46.4	46.4 dB
Carrier S/N required for tracking	9 dB	
Tracking bandwidth, 200 Hz	23	
Minimum carrier power/noise, P_C/N_O	32	
Signal energy/noise, $P_e = 10^{-3}$	10.8	
Data rate, 100 bits/sec	20	
Minimum signal power/noise, P_S/N_O	30.8	
Minimum signal/noise, $P_r/N_O = (P_C/N_O) + (P_S/N_O)$	34.4	
Margin for equipment tolerance	3.0	
Threshold signal/noise	37.4	-37.4
Relay link margin		9.0 dB

TABLE 8.- PROBE WEIGHT AND POWER

	Weight, kg	Power, W
Science	7.3	17.3
Data subsystem and timer	3.6	5
Transmitter	2.7	327
Antenna	2.7	---
Receiver and command	1.4	1
Cabling and mounting	8.6	---
Batteries and regulation	27	---
Pressure shell	46	---
Aeroshell support structure	33	
Heat shield	110	
Entry weight	242	
Total power		355.3
Spin-up motor and gas	4	
Probe weight (deflected bus)	246	
Deflection propulsion	46	
Probe weight (deflected probe)	292	

TABLE 9.- BUS TO EARTH TELEMETRY LINK

Spacecraft effective radiated power			ERP, dB
Transmission loss	-2.0	dB	
Pointing loss	-0.5		
Free space loss, 5.6 a.u.	-278.2		
Receiving antenna gain, 210 ft	61.4		
Loss in received power	-219.3	dB	-219.3
Carrier channel requirements			
Modulation loss			-6.9
Carrier power			-226.2
Noise	-202.4	dB	
Signal/noise threshold	6.0		
Margin	3.0		
Carrier threshold	-193.4	dB	193.4
Excess carrier margin			-32.8
Data channel requirements			
Modulation loss			-1.0
Subcarrier power			-220.3
Noise	-213.2	dB	
Signal/noise threshold	4.1		
Margin	3.8		
Subcarrier threshold	-205.3	dB	205.3
Excess subcarrier margin			-15.0

TABLE 10.– TOTAL SPACECRAFT WEIGHT

	(a) Deflected probe				(b) Deflected bus			
	Baseline science		Complete science		Baseline science		Complete science	
Data rate, bits/sec	800	8500	800	9000	800	8500	800	9000
Science instruments, kg	24	24	60	60	24	24	60	60
Scan platform, kg	15	15	28	28	15	15	28	28
Relay radio and data, kg	9	9	9	9	9	9	9	9
Relay antenna and tracking, kg	27	27	27	27	27	27	27	27
Data handling, kg	23	23	23	23	23	23	23	23
Recorders, kg	14	14	14	14	14	14	14	14
Transmitter, kg	5	13	5	13	5	13	5	13
Radio/sequencer, kg	36	47	43	55	36	47	43	55
Earth link antenna, kg	14	17	14	17	14	17	14	17
Structure, kg	125	191	167	235	126	192	168	236
Cabling, kg	42	63	55	77	42	63	55	77
Attitude control, kg	28	34	30	36	29	35	31	38
Power, kg	130	269	176	320	130	269	176	320
Propulsion, kg	29	39	35	45	165	222	201	260
Probe mounting, kg	16	16	16	16	16	16	16	16
Bus total (excluding probe), kg	537	801	702	975	675	986	870	1193
Deflected probe weight, kg	292	292	292	292	246	246	246	246
Total system weight	829	1093	994	1267	921	1232	1116	1439

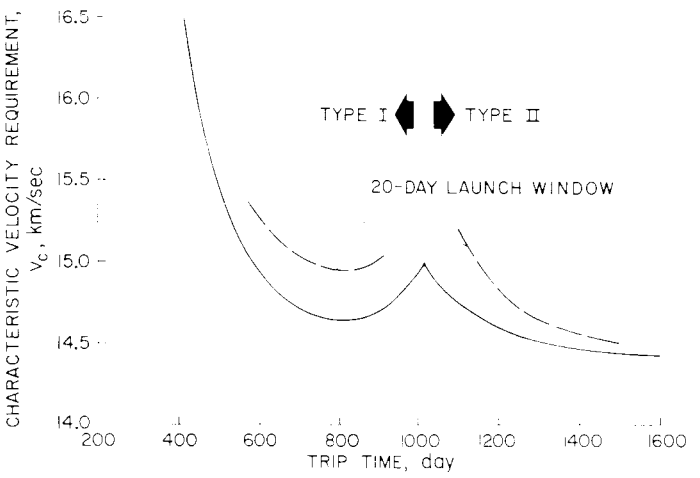

(a) 1978 opposition.

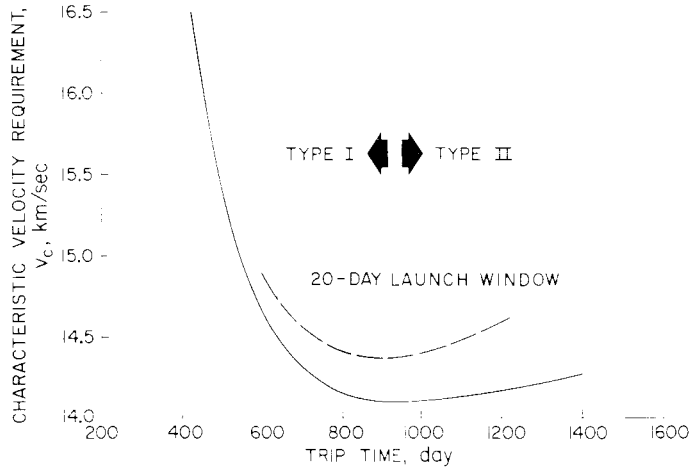

(b) 1981 opposition.

Figure 1.– Characteristic velocity requirements.

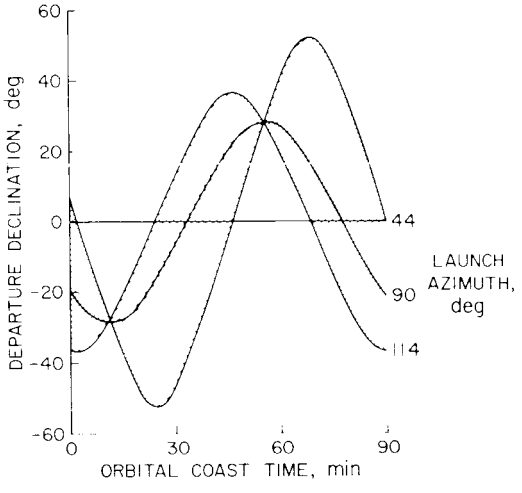

Figure 2.- Orbital coast time requirements for departure.

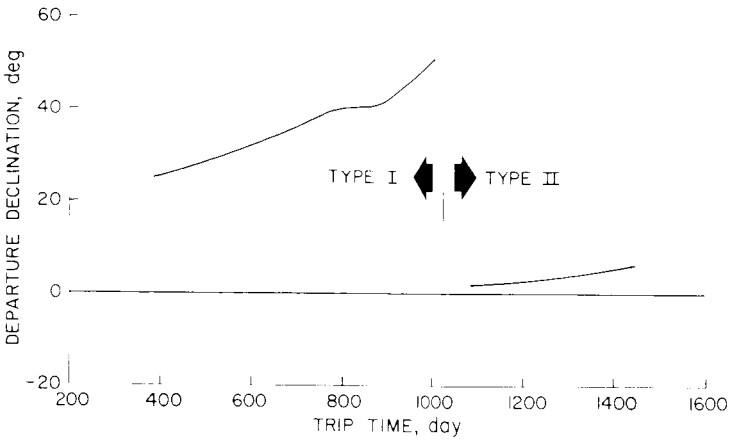

(a) 1978 opposition.

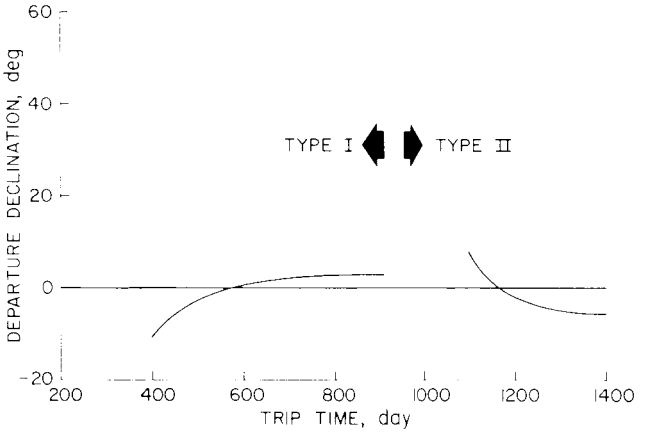

(b) 1981 opposition.

Figure 3.– Departure declination.

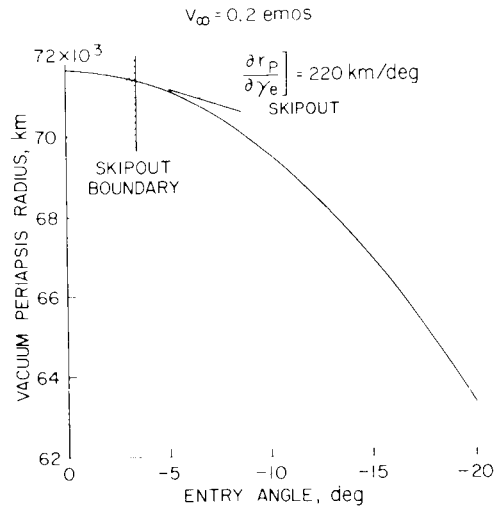

Figure 4.– Vacuum periapsis radius for entry.

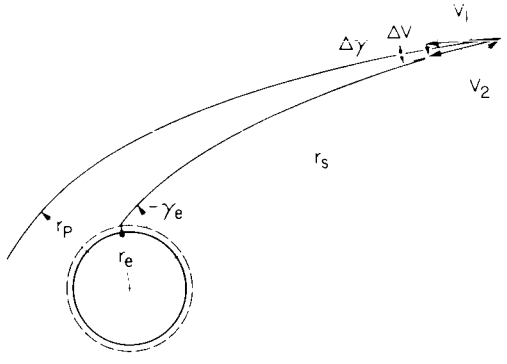

Figure 5.– Separation schematic – deflected probe.

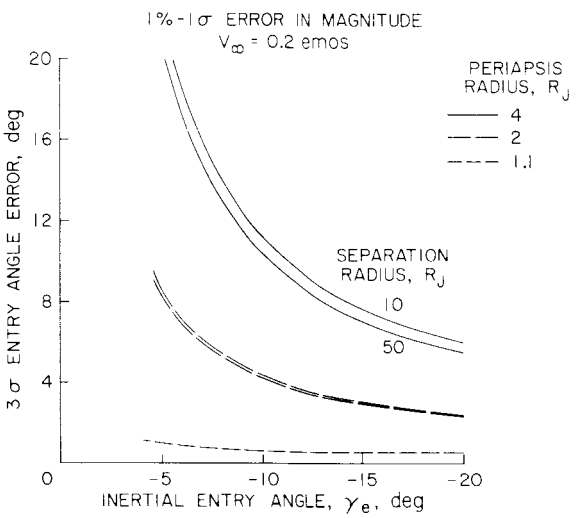

Figure 6.– Entry angle errors due to separation increment magnitude error.

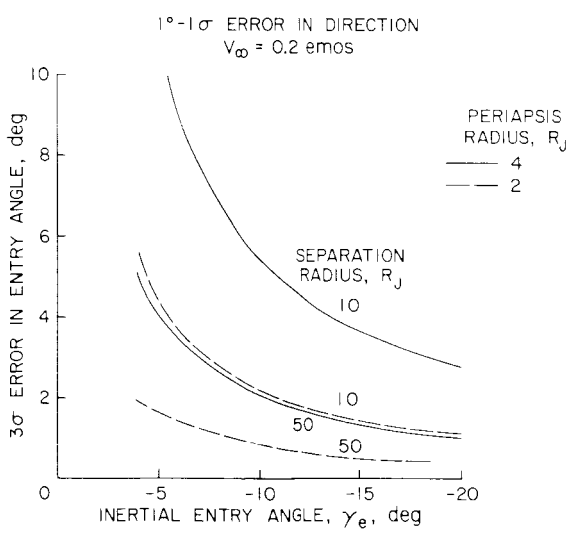

Figure 7.– Entry angle errors due to separation increment direction error.

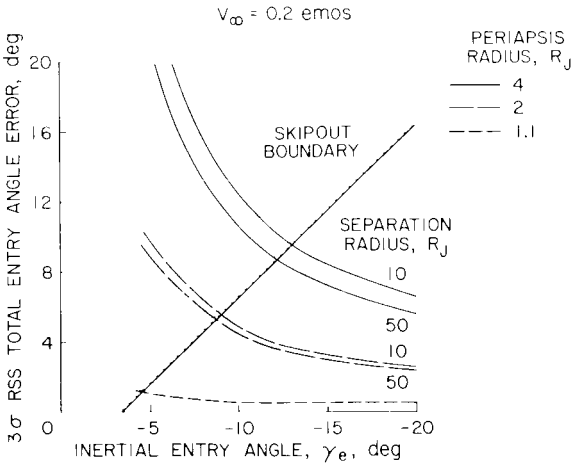

Figure 8.– Total entry angle error.

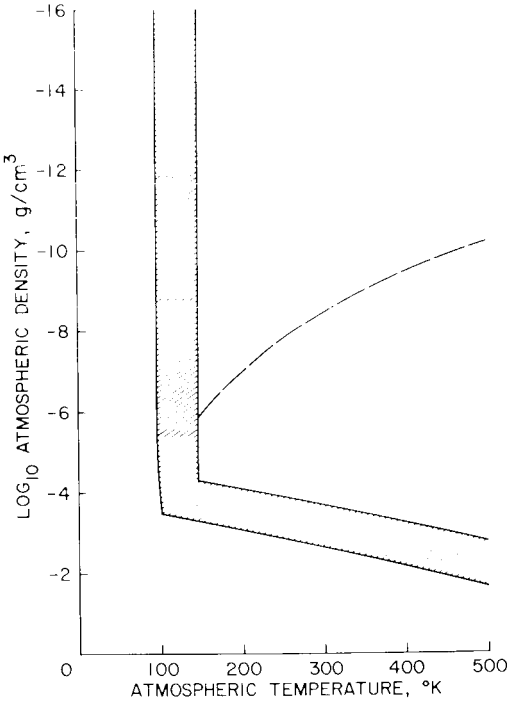

Figure 9.– Atmosphere uncertainties.

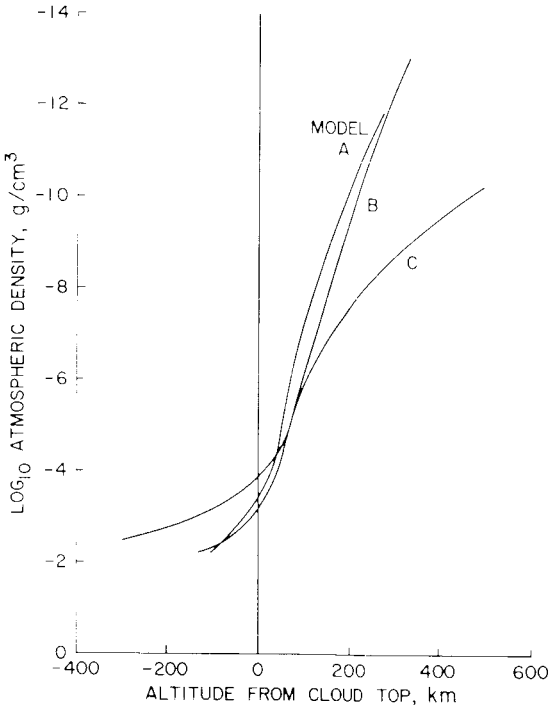

Figure 10.-- Atmosphere models.

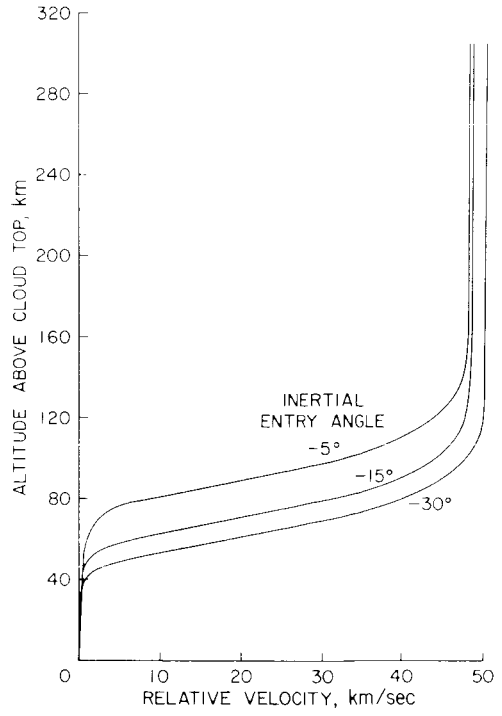

Figure 11.-- Entry altitude -- velocity profiles.

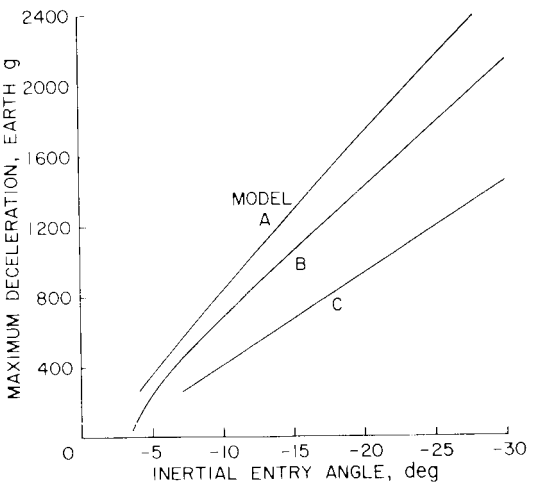

Figure 12.– Maximum deceleration during entry.

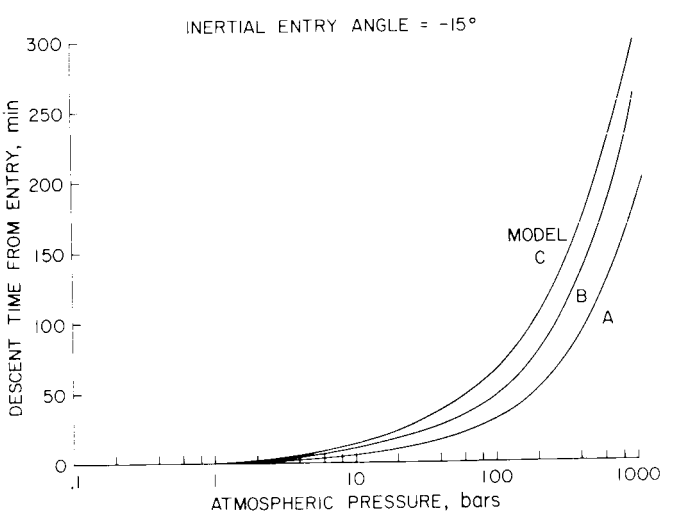

Figure 13.– Descent time required to reach various pressure levels.

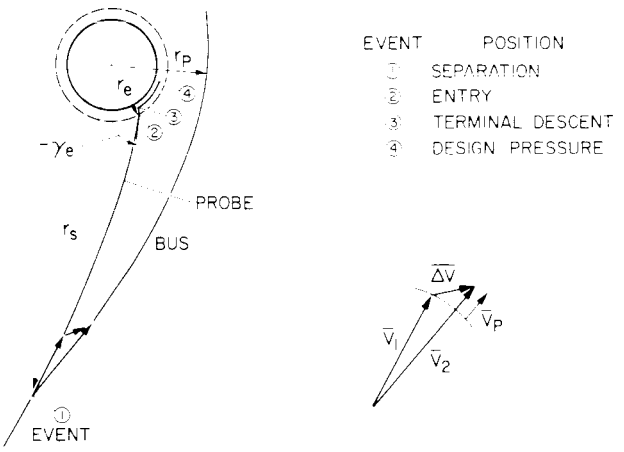

(a) Deflected bus.

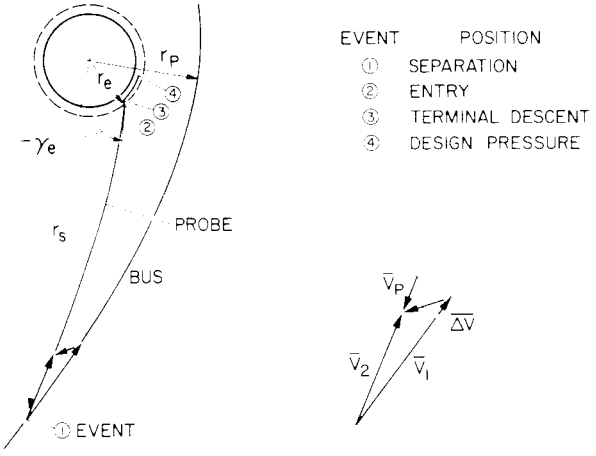

(b) Deflected probe.

Figure 14.– Separation geometry.

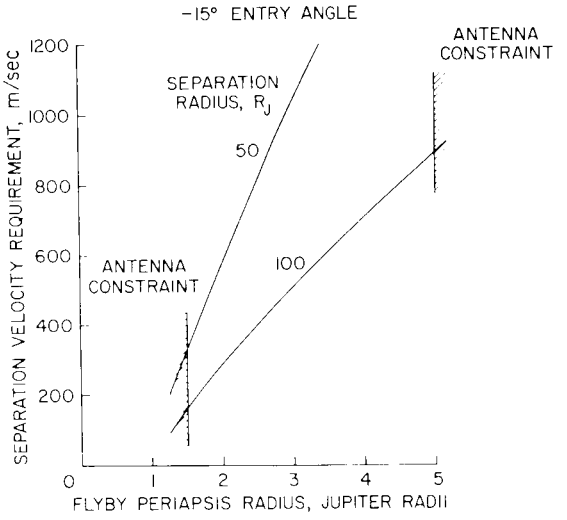

(a) $\gamma_e = -15°$

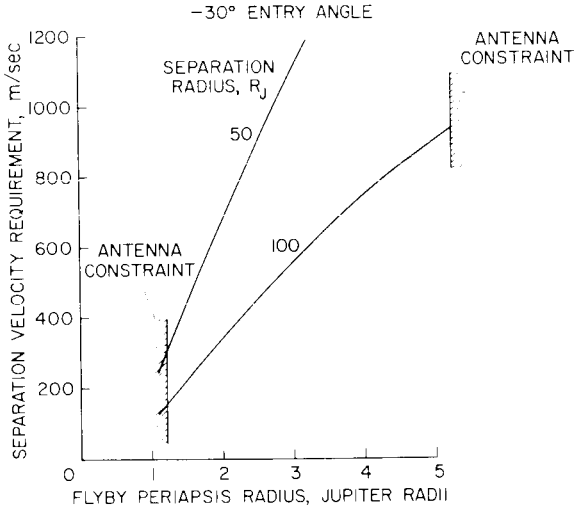

(b) $\gamma_e = -30°$

Figure 15.– Separation velocity requirements for deflected bus and deflected probe.

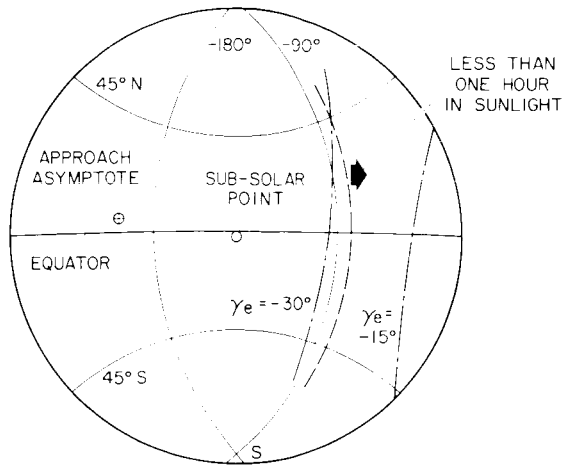

(a) 1978 800-day trip.

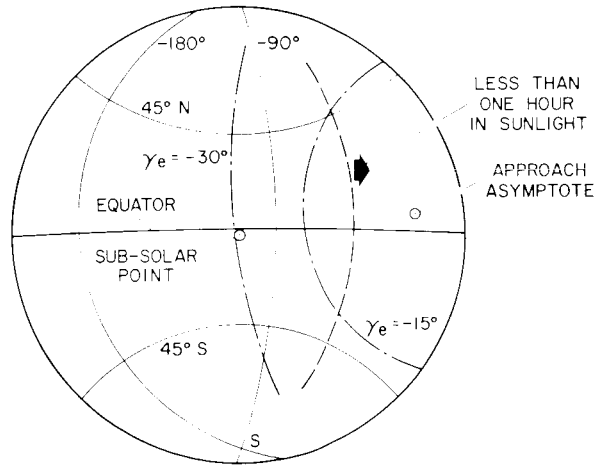

(b) 1978 1200-day trip.

Figure 16.– Stereographic projection of planetary encounter.

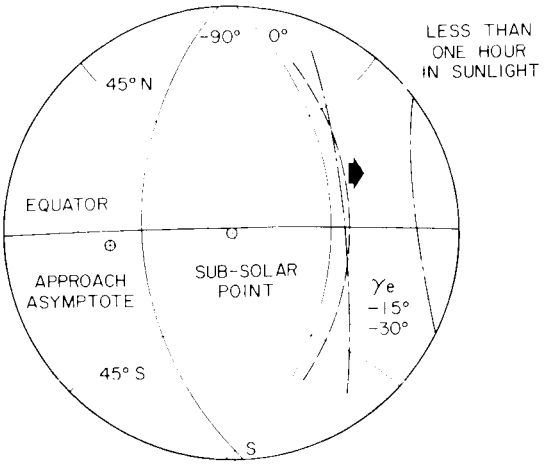

(c) 1981 800-day trip.

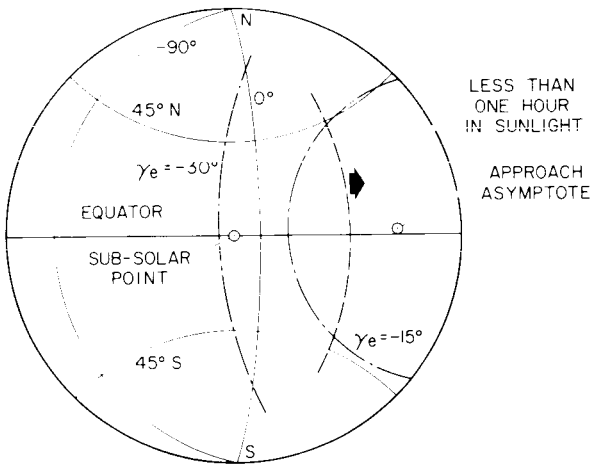

(d) 1981 1200-day trip.

Figure 16.— Concluded.

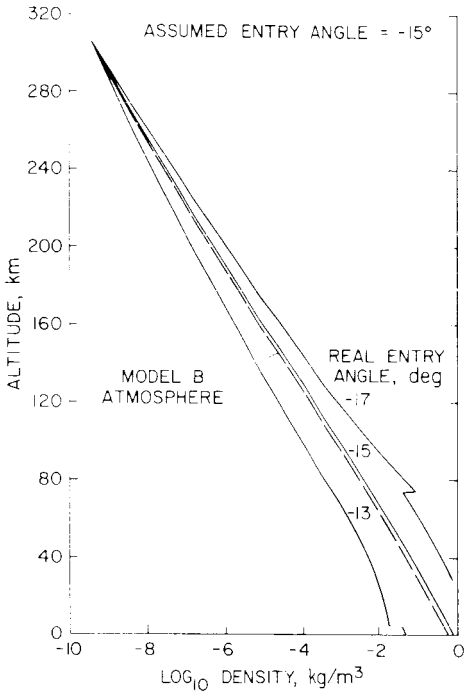

(a) $\gamma_e = -15°$

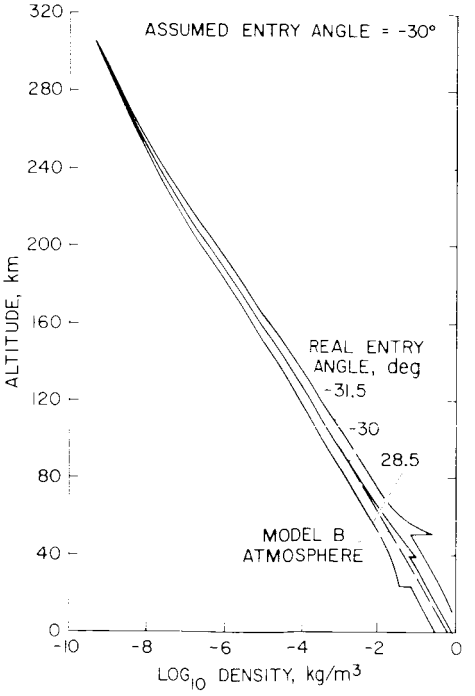

(b) $\gamma_e = -30°$

Figure 17.– Atmospheric reconstruction uncertainties due to entry angle errors.

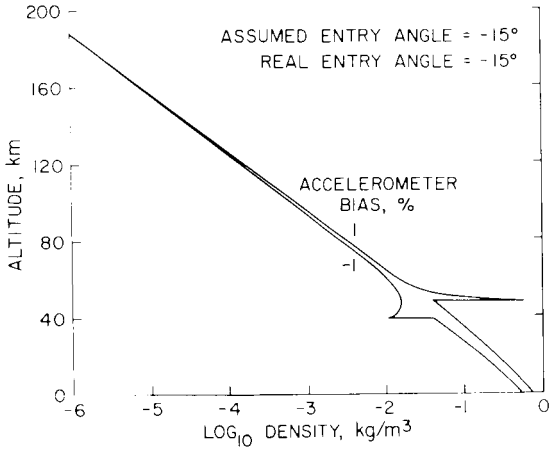

(a) $\gamma_e = -15°$

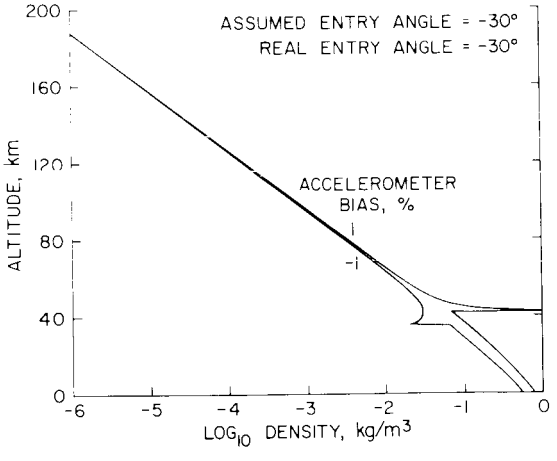

(b) $\gamma_e = -30°$

Figure 18.– Atmospheric reconstruction uncertainties due to accelerometer bias errors.

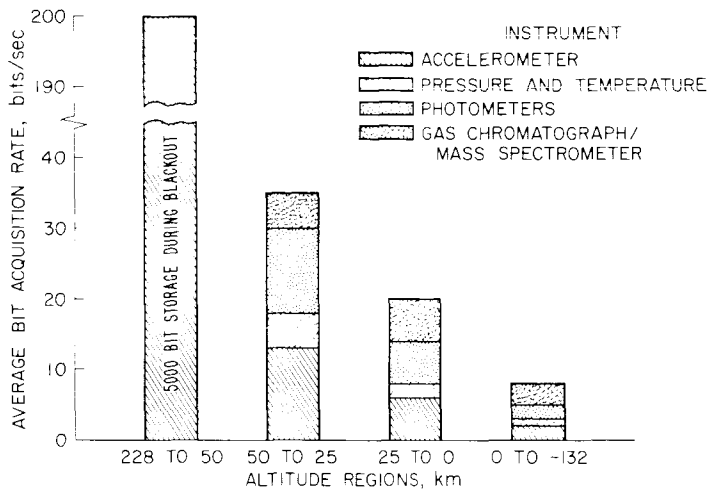

Figure 19.– Probe data acquisition.

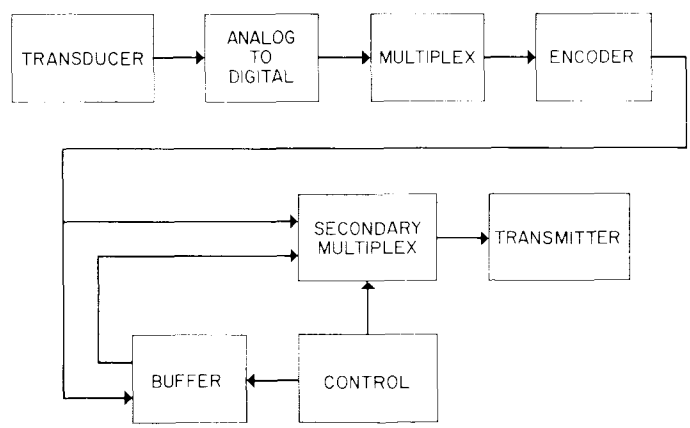

Figure 20.– Probe data handling.

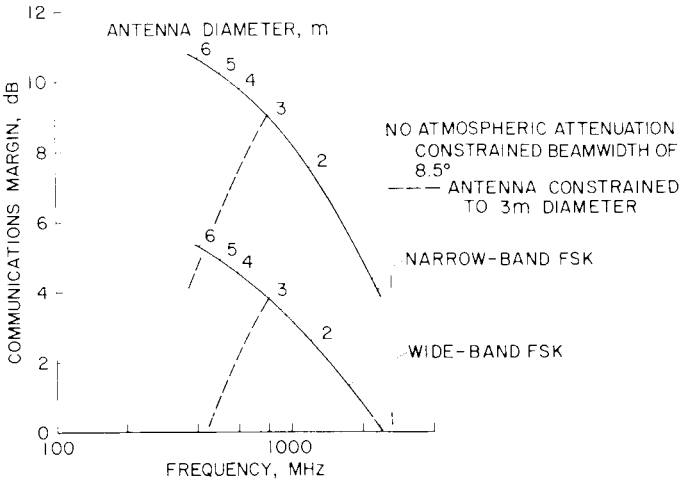

Figure 21.– Probe communications margin excluding attenuation.

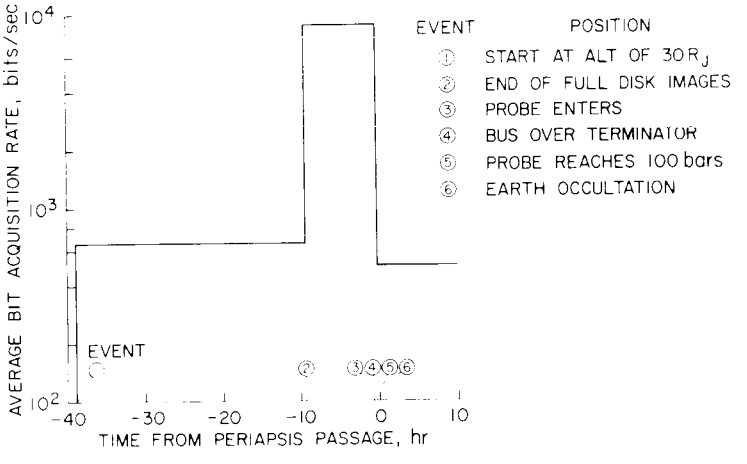

Figure 22. Bus data acquisition.

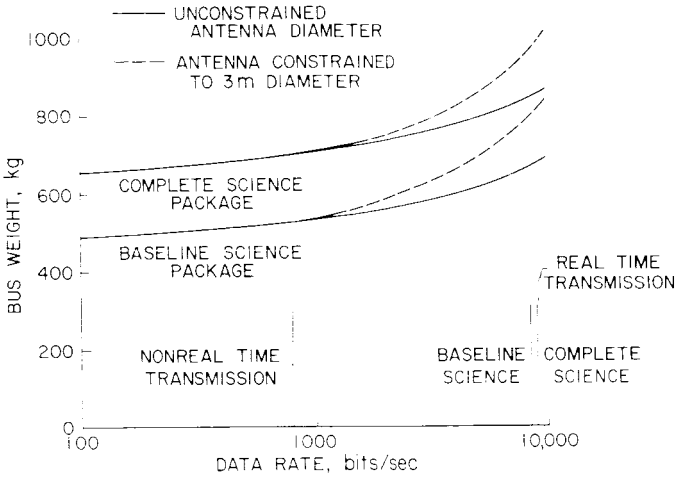

Figure 23.– Bus weight comparisons.

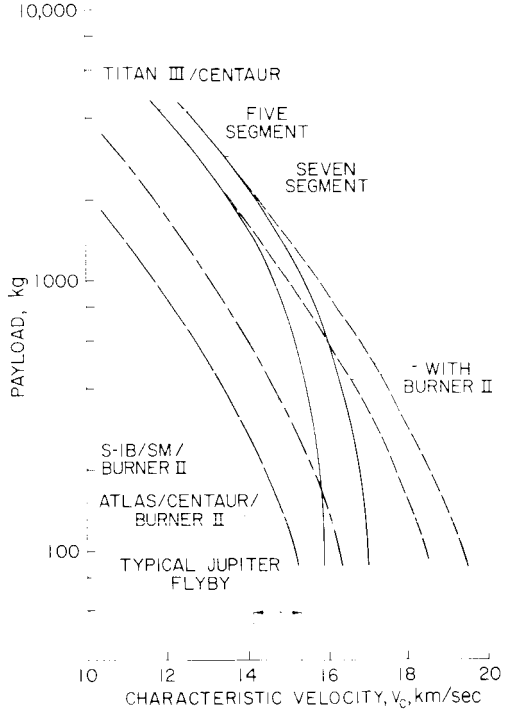

Figure 24.– Booster payload capabilities.

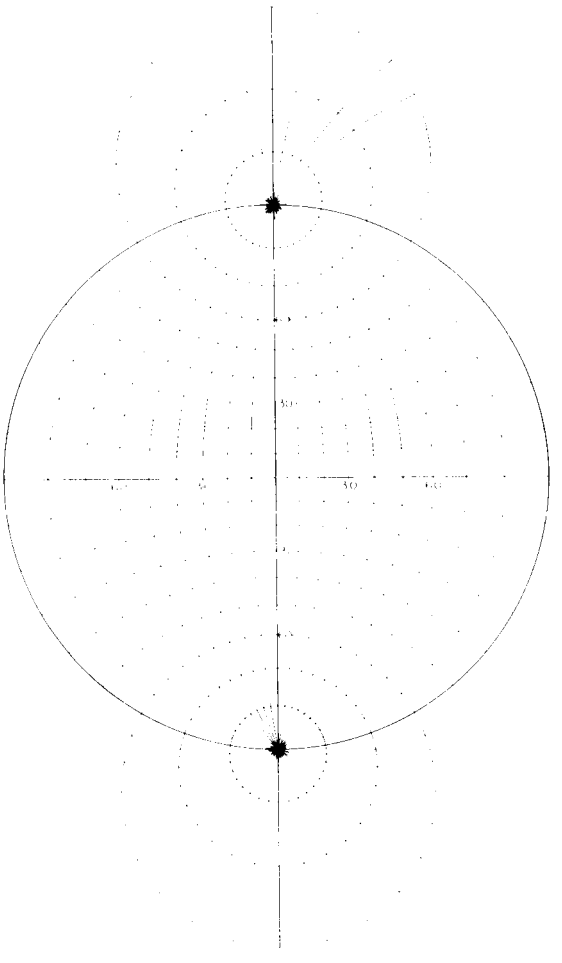

Figure 25.– Stereographic projection overlay.

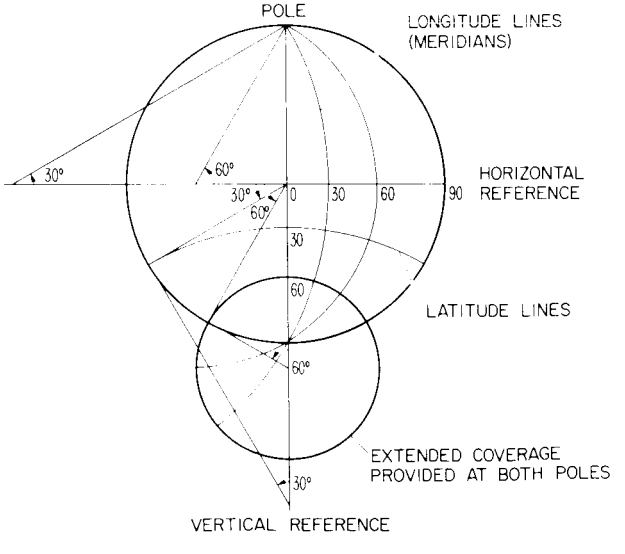

Figure 26.– Overlay construction.

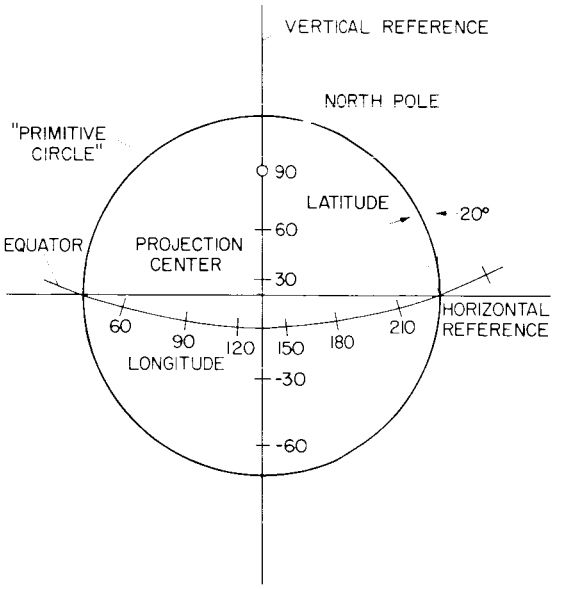

Figure 27.– Projection coordinates.

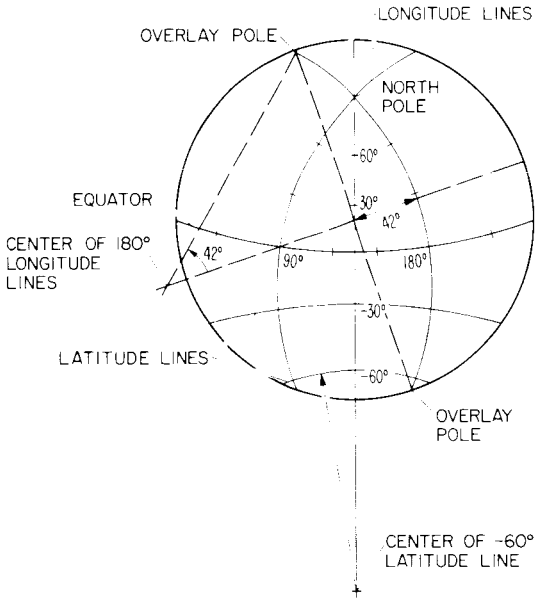

Figure 28. – Longitude and latitude construction.

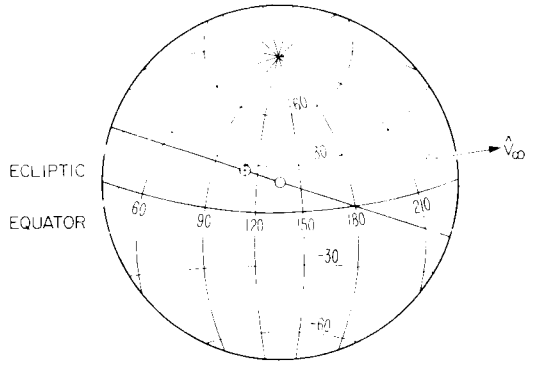

Figure 29. Arrival conditions display.

NASA-Langley, 1971 — 30 A-3826